56p.

N63 19652

Code-1

NASA

TECHNICAL NOTE

D-1807

WIND-TUNNEL MEASUREMENT OF PROPELLER WHIRL-FLUTTER

SPEEDS AND STATIC-STABILITY DERIVATIVES AND

COMPARISON WITH THEORY

By Samuel R. Bland and Robert M. Bennett

Langley Research Center
Langley Station, Hampton, Va.

NATIONAL AERONAUTICS AND SPACE ADMINISTRATION

WASHINGTON   August 1963

NATIONAL AERONAUTICS AND SPACE ADMINISTRATION

TECHNICAL NOTE D-1807

WIND-TUNNEL MEASUREMENT OF PROPELLER WHIRL-FLUTTER

SPEEDS AND STATIC-STABILITY DERIVATIVES AND

COMPARISON WITH THEORY

By Samuel R. Bland and Robert M. Bennett

SUMMARY

    Results of an experimental investigation of propeller whirl flutter are
presented for a model consisting of an isolated, rigid system of propeller and
simulated power plant mounted with flexibility in pitch and yaw on a rigid sting.
A range of propeller blade angles, restraint stiffnesses, and restraint damping
coefficients was investigated for a system symmetrical in pitch and yaw with a
windmilling propeller. Measurements of the static-stability derivatives were
also made by using a simple balance and were compared with two sets of theoretical
derivatives. Whirl-flutter calculations were made with the theoretical and meas-
ured derivatives. Some limited results were obtained for the whirl flutter of
the model mounted on a cantilever semispan wing.

    The measured whirl-flutter speeds and frequencies of the isolated model were
in very good agreement with those predicted by calculations in which measured
derivatives and viscous damping were used. This agreement was better than that
obtained by using structural damping. Predicted whirl-flutter speeds for the
isolated model were lower when theoretical stability derivatives were used than
when measured derivatives were used. The theoretical and experimental static-
stability derivatives exhibited the same trends, but in certain instances dif-
fered appreciably in magnitude. There was little effect of the semispan wing on
the measured whirl-flutter boundary for the one configuration considered.

INTRODUCTION

    It is well known that a combination of propeller and power plant can develop
a dynamic instability, generally termed propeller whirl flutter or autoprecession,
in which the hub wobbles or executes a whirling motion. In several analytical
investigations (refs. 1 to 4) the flutter boundaries of an isolated nacelle have
been investigated by developing the equations of motion with calculated stability
derivatives for the aerodynamics of the propeller, and by making parametric trend
studies from these equations. However, there have been no comparable experimental
data available for verification of these analytical studies. For example, in

reference 2 a comparison of the theoretical results with the flutter data for a four-engine model showed comparable trends but poor quantitative agreement, perhaps as a result of the effects of the complete model on the whirl-flutter boundaries. Therefore, the present investigation was undertaken with two objectives:

1. To obtain experimental whirl-flutter boundaries on a simple system that is readily amenable to analysis, in order to evaluate existing propeller-whirl theories.

2. To measure, on the same system, some of the propeller aerodynamic derivatives required to predict whirl flutter, in order to evaluate methods for calculating the stability derivatives of the propeller.

Also, the effects of a wing on the flutter boundary are indicated by a comparison with some limited results obtained with the model mounted on a cantilever semispan wing.

Measurements of the static aerodynamic stability derivatives of the windmilling propeller were made by using a simple balance and were compared with the theory of reference 3 and the theory of reference 5 as applied in reference 2. Whirl-flutter speeds and frequencies were measured for a combination of a windmilling propeller and simulated power plant which was mounted on a sting by means of a spring-restrained gimbal. A range of propeller blade angles, restraint stiffnesses, and restraint damping coefficients was investigated for a system symmetrical in pitch and yaw. Whirl-flutter calculations made with both sets of theoretical derivatives (theories of refs. 3 and 5) and measured derivatives were compared with experiment.

<div align="center">SYMBOLS</div>

A   propeller-blade aspect ratio

b   propeller-blade section chord, ft

C_m pitching-moment coefficient, $\dfrac{\text{Pitching moment}}{qSD}$

C_m^* total pitching-moment coefficient, $\quad C_m - \dfrac{l}{2R} C_Z$

C_n yawing-moment coefficient, $\dfrac{\text{Yawing moment}}{qSD}$

C_n^* total yawing-moment coefficient, $\quad C_n + \dfrac{l}{2R} C_Y$

C_n^{**} total yawing-moment coefficient including effect of yaw strain-gage beam deflection (see eq. (A7))

C_Y side-force coefficient, $\dfrac{\text{Side force}}{qS}$

C_Z vertical-force coefficient, $\dfrac{\text{Vertical force}}{qS}$

c_{l_α} section lift-curve slope of propeller blade

D propeller diameter, ft

f vibration frequency, cps

g structural damping coefficient

$\bar{g}$ average structural damping coefficient, $\dfrac{g_\theta + g_\psi}{2} \dfrac{\rho_o}{\rho}$

H moment-of-inertia ratio, $\dfrac{\pi I_X}{I_Y}$

I_X mass moment of inertia of propeller about axis of rotation, slug-ft^2

I_Y mass moment of inertia of propeller-engine system about pitch axis, slug-ft^2

J propeller advance ratio, $\dfrac{V}{nD}$

K rotational stiffness of engine-propeller system, ft-lb/radian

k reduced frequency of engine-propeller system, $\dfrac{R\bar{\omega}}{V}$

l distance from plane of propeller-blade quarter-chord points at three-quarter radius to gimbal axes, $l_o + \dfrac{b_{0.75R}}{4} \sin \beta_{0.75R}$, ft

l_o distance from plane of propeller-blade midchord line to gimbal axes, ft

M free-stream Mach number

n propeller rotational speed, rps

q free-stream dynamic pressure, lb/sq ft

R propeller radius, ft

S propeller disk area, πR^2, sq ft

t	time, sec
V	free-stream velocity, ft/sec
x	distance along propeller blade, fraction of R
β	propeller geometric blade angle measured from plane of propeller rotation, deg
β_0	propeller blade angle for zero lift measured from plane of propeller rotation, deg
δ	lag angle of oscillatory aerodynamic forces, deg
ζ	viscous-damping coefficient, ratio of viscous damping to critical damping
$\bar{\zeta}$	average viscous-damping coefficient, $\dfrac{\zeta_\theta + \zeta_\psi}{2}\dfrac{\rho_0}{\rho}$
θ	pitch angle of propeller-shaft axis
κ	density-inertia ratio, $\dfrac{\pi\rho R^5}{I_Y}$
λ	frequency ratio, $\dfrac{\omega_f}{\bar{\omega}}$
ρ	air density, slugs/cu ft
ρ_0	reference air density, 0.0022 slug/cu ft
σ	propeller solidity at three-quarter radius, $\dfrac{8b_{0.75R}}{3\pi R}$ (for four-blade propeller)
τ	nondimensional distance traveled in propeller radii, $\dfrac{Vt}{R}$
ψ	yaw angle of propeller-shaft axis
Ω	propeller rotational speed, radians/sec
ω	frequency, radians/sec
$\bar{\omega}$	average wind-off frequency, $\dfrac{\omega_\theta + \omega_\psi}{2}$, radians/sec

Subscripts:

0.75R   three-quarter propeller radius

f   condition at whirl flutter

i = 1,2,3   wing vibration modes

q   differentiation with respect to θ'

r   differentiation with respect to ψ'

θ pitch direction

ψ yaw direction

Primes denote differentiation with respect to τ.

Partial derivatives are denoted by double subscripts; for example:

$$C_{m_\theta} = \frac{\partial C_m}{\partial \theta}, \quad C_{m_q} = \frac{\partial C_m}{\partial q}, \text{ and so forth.}$$

APPARATUS

Tunnel

The Langley transonic dynamics tunnel is a slotted-throat, variable-pressure, single-return wind tunnel having a test section 16 feet square (with cropped corners). It is capable of operation at Mach numbers up to 1.2 and at stagnation pressures from near vacuum to slightly above atmospheric. Either air or Freon-12 can be used as a test medium. Large windows are provided for close, unobstructed viewing of the model.

Models

The isolated model consisted of a combination of simulated engine mass and propeller attached to a steel mounting beam through a gimbal with pitch and yaw freedoms. The engine-propeller system was elastically restrained for pitch and yaw movements with a steel spring. The steel mounting beam was bolted to a sting on the wind-tunnel center line. A balsa nacelle cover, similar to one type of present-day turboprop nacelle, covered the gimbal, propeller shaft, and engine. This nacelle was faired at its after end into an aluminum cylinder which covered the end of the sting. Figure 1 is a photograph of the model in the tunnel. Two propeller-shaft lengths (shown in fig. 2) were used. Details of the method of spring restraint and the gimbal arrangement, which differed for the models used in the whirl and derivative tests, are given subsequently.

The whirl-flutter model was also mounted on a cantilever semispan wing as shown in figure 3.

Propeller.- The four-blade aluminum propeller used in these tests was a 1/8-scale model of that treated in reference 2 and was typical of the type used on turboprop aircraft; however, the propeller did not have blade-root cuffs. Figure 4 gives the blade width and twist distributions. Figure 5 presents the variation of windmilling-propeller advance ratio with blade angle at the three-quarter-radius station as found in this test. The propeller blade frequencies, with the hub rigidly clamped, were as follows: First bending, 172 cps; first chordwise bending, 296 cps; second bending, 567 cps; first torsion, 1,105 cps. There was little change in the frequency of the first mode with the propeller mounted on the model.

Isolated whirl model.- Figure 6 is a photograph of the whirl model with the cover removed; the model is shown schematically in figure 7(a). The gimbal allowed the propeller-engine system freedom to pitch and yaw. The spring restraint was a hardened piece of 1/4-inch-diameter drill rod, screwed into the rear of the propeller shaft housing on the center line of the shaft axis. The opposite (rearward) end of the spring passed through a hole in the steel clip that could be screwed to the mounting beam at several locations to provide variations in stiffness. This arrangement provided equal stiffness in all directions. A variable-speed motor with an eccentrically mounted weight on its shaft formed part of the engine mass and served as a shaker device.

The measured physical properties of the model are given in table I. Measured values of spring stiffness agreed with values calculated from the measured moments of inertia and frequencies to within 5 percent. The pitch and yaw natural frequencies (propeller not rotating) ranged from 7.6 to 11.5 cps. The amount of damping in the system was adjusted by inserting sponge rubber between the gimbal rings (fig. 6). Figure 8 shows four typical samples of the data reduced from decay records that were obtained by locking out one degree of gimbal freedom, deflecting the propeller shaft, and releasing it. In two of the cases presented the damping is reasonably independent of amplitude (constant slope); in the other cases there is an increase in damping with increasing amplitude.

For the whirl tests, the sting was restrained by cables attached to its upstream end. (See figs. 1 and 6.) The sting stiffness was about one hundred times the stiffness of the propeller-engine system. The sting pitch frequency with the model and cables in place was 23 cps; the yaw frequency was 20 cps.

Derivative model.- The isolated whirl-flutter model was modified in several ways for use in the derivative measurements. One direction of gimbal freedom was locked out so that the gimbal became essentially a single pivot and allowed motions in one plane only as shown in figure 7(b). Also, a flat spring was used as a strain-gage beam bolted at its forward end to the propeller housing and clamped at its rearward end to a flexible steel clip bolted to the mounting beam. The mounting beam could be bolted to the sting in such a manner as to allow either pitch or yaw freedom in the tunnel (fig. 7(b)).

It was impractical to restrain the sting with cables during the derivative tests, as the end of the sting translated somewhat when the sting angle was varied to determine the static derivatives. The sting stiffness was about twenty-five times the spring stiffness, and its frequency with the model in place was about 14 cps.

Wing-mounted model.- The propeller and gimbal arrangement for the whirl-flutter model was mounted on a cantilever semispan wing. The general arrangement and the wing modal frequencies and node lines are indicated in figure 9. The wing was adapted from that of the four-engine model of reference 6. It consisted of a built-up aluminum spar for stiffness and balsa pods for airfoil contour.

Instrumentation

Tunnel static and stagnation pressures were measured with manometers and were recorded in digital form, with stagnation temperature, on manual command at each data point by means of the tunnel automatic-readout system.

The angular accelerations about the gimbal axes of the propeller whirl model were determined by linear accelerometers mounted on the simulated engine mass as shown in figure 6, and were recorded on a direct-writing oscillograph recorder. Propeller rotational speed was measured by a magnetic pickup mounted at the propeller shaft and driving an electronic counter.

In the stability-derivative tests, the moment about the gimbal axis was sensed by strain gages on the gimbal restraining spring. The signal from the strain gage was read out on a fixed-gain, digital voltmeter, and printed out in digital form. Propeller angle of attack was measured by a $\frac{1}{2}g$ accelerometer mounted on the simulated engine mass (fig. 7(b)). The mean value of the accelerometer signal was recorded in a manner similar to that for the moment signal. The sting angle was also measured by a calibrated counter on the actuator mechanism and was recorded manually.

TESTS

Whirl-Flutter Tests

The linear theory of the stability of the whirl mode (refs. 2 and 3) indicates that there is a critical speed at which a disturbance of the mode will produce constant-amplitude oscillations; at lower speeds the mode would be stable and at higher speeds the mode would be unstable. In the tests of the whirl-flutter model, the tunnel was brought up to a low speed, the model was disturbed by the shaker, and the stability of the response was observed visually and on the oscillograph record. Airstream velocity was then increased by a small increment, and the model was again disturbed. This procedure was continued

until a sustained, approximately constant amplitude oscillation was produced. The tunnel conditions were then recorded as the conditions for flutter.

In some cases, the stability of the whirl mode was related to velocity as indicated by linear theory; however, in many of the tests there was no such sharply defined flutter speed. In the latter cases the amplitude of flutter was limited for a given velocity and increased with an increase in velocity, indicating a nonlinear effect. These configurations corresponded to those having a damping that increased with amplitude (fig. 8). For these configurations, velocity was increased until the amplitude of oscillation was about 3° or 4°, and the tunnel conditions were then recorded as the conditions for flutter. The pertinent damping coefficient used in this report for these cases was assumed to be that derived from the slope of the decay records (fig. 8) at the amplitude of flutter. Damping records were taken before and after a series of runs for each stiffness or damping level.

All the whirl-flutter tests were made in air at near atmospheric conditions and low Mach numbers ($M \leqq 0.25$).

Derivative Tests

The moment about the gimbal axis was measured over a wide range of pitch angle θ by varying the angle of the sting. Two distances between the gimbal axis and propeller plane were used $\left(\dfrac{l_o}{R} = 0.346 \text{ and } \dfrac{l_o}{R} = 0.691\right)$ in order to separate the force and moment contributions to the total moment. The method of obtaining the stability derivatives from the slopes of the total-moment-coefficient curves is given in appendix A.

At low Mach numbers ($M \leqq 0.26$) the moment about the gimbal axis was measured with $\beta_{0.75R} = 25^o$, 35°, 46°, 52°, and 58°, with both shaft lengths, and with the gimbal axis oriented for pitching-moment measurements and for yawing-moment measurements. The nominal value of dynamic pressure was either 50 or 100 pounds per square foot. In addition, measurements were made for $\beta_{0.75R} = 58^o$, and $\dfrac{l_o}{R} = 0.346$ with the gimbal oriented for pitch measurements at Mach numbers of 0.90, 0.70, and 0.48 and oriented for yaw measurements at Mach numbers of 0.90 and 0.70. A nominal value of dynamic pressure of 100 pounds per square foot was maintained at the higher Mach numbers by varying the static pressure within the tunnel.

During some of the derivative tests a mild oscillation of limited amplitude was encountered. In some cases it occurred only at the higher angles of attack, and in others at the higher values of dynamic pressure. These oscillations had no apparent effect on the measurement of the static derivatives, since such measurements depend primarily on the mean values of the measured quantities. Attempts were made to measure the damping derivative C_{m_q} by obtaining decay records after a shaker disturbance at several airstream velocities for a system with a weak

pitch spring and no yaw freedom. However, again limited-amplitude oscillations were obtained, and thus C_{m_q} could not be determined in a simple manner by using the equation for a single degree of freedom. (A method of estimating C_{m_q} from whirl-flutter speeds is described subsequently.) The ratio of pitch to yaw stiffness for this condition (sting tied down with cables) was approximately 1 to 100, whereas for the static derivative tests (sting not tied down with cables) the stiffness ratio was approximately 1 to 25. The linear two-degree-of-freedom analysis of reference 2 for a pivoting simple system does not predict an instability at the speeds of the derivative tests for the stiffnesses involved, and the explanation of these limited-amplitude oscillations is unknown at the present time.

RESULTS AND DISCUSSION

Presentation of Results

The results are presented and discussed in three parts. First, the theoretical and experimental stability derivatives are considered (figs. 10 to 13) because they are required as an input for the whirl-flutter calculations. Second, the measured and calculated whirl-flutter boundaries and frequencies for the isolated nacelle are considered (figs. 14 to 20 and table II). Third, some wing effects are discussed by comparing the measured flutter boundaries for the isolated nacelle with limited results for the wing-mounted nacelle (fig. 21 and table II).

Propeller Stability Derivatives

The experimentally determined static-stability derivatives ($M \leq 0.26$) are compared in figure 10 with derivatives calculated by the method of reference 5 (incorporating the lag terms of ref. 2), and with the strip theory of reference 3. The derivatives of figure 10 are derived from the faired curves of figure 11 by means of equations (A4), (A5), (A9), and (A10) of appendix A. The theoretical values of C_{m_θ} (fig. 10(c)) were computed from $C_{m_\psi} \tan \delta$, which can be derived in a manner similar to the derivation of C_{Z_ψ} in reference 2. As previously discussed, no experimental values of C_{m_q} were determined.

Application of theory.- In the application of the theory of reference 5 to the windmilling propeller, the effective local helix angle was assumed to be given by $V/\Omega Rx$. That is, momentum losses and interactions between the blades were assumed to be negligible. A section lift-curve slope of 2π, fineness ratio of 6.0 for the spinner-nacelle combination, and a ratio of spinner radius to propeller radius of 0.181 were used in evaluating the integrals over the portion of the blade having lifting sections (outer three-quarters of the radius).

The derivatives calculated by the theory of reference 3 for windmilling propellers are somewhat simpler to evaluate than those of the theory of

reference 5. Since these derivatives are directly proportional to c_{l_α}, the aspect-ratio correction factor $\frac{A}{A+2}$ (developed for wings) was used as suggested in reference 3. Evaluating A over the outer three-quarters of the radius yields a value of 3.47 for A and a correction factor of 0.635. The integrals of this method (eqs. (B9) of ref. 3) were also evaluated over the outer three-quarters of the radius.

Comparison of theory and experiment.- In general, the trends of the theoretical derivatives correspond to the experimental trends, but the magnitudes differ considerably in certain cases. The values of C_{Z_θ} (fig. 10(a)) predicted by the method of reference 5 are about 25 percent larger than the experimental ones, while the values predicted by the method of reference 3 are in agreement at low blade angles but are smaller by 15 percent at the higher blade angles. In references 5 and 7 the data cited were within ±10 percent of values of C_{Z_θ} calculated by the method of reference 5. The difference in the present case might be attributed to experimental inaccuracy (estimated to be ±10 percent), to the value 2π used for section lift-curve slope (section data were not available for this propeller), or to the peculiar geometry of the inboard portion of the propeller.

The values of C_{m_q} (fig. 10(a)) computed from the two theories have the same trend, but the values predicted by the theory of reference 3 are somewhat smaller. Both theories give results for C_{m_ψ} that are in good-to-fair agreement with experimental results over the blade-angle range (fig. 10(b)), but are 2 to 20 percent higher. The experimental accuracy of this derivative is estimated to be approximately ±10 percent also.

The theoretical values of C_{Z_ψ} and C_{m_θ} (fig. 10(c)) are lower than experiment and are in fair-to-poor agreement. The estimated experimental accuracy is about ±10 percent for C_{m_θ} and ±25 percent for C_{Z_ψ}. The theoretical expressions for C_{m_θ} and C_{Z_ψ} $\left(C_{m_\theta} = C_{m_\psi} \tan \delta; \; C_{Z_\psi} = -C_{Z_\theta} \tan \delta \right)$, as applied in references 2 and 3, are approximations and would not be expected to yield accurate results.

A further indication of the error in the unsteady-flow lift-lag phase angle δ, as obtained in references 2 and 3, can be seen in figure 12 by comparing the phase angles derived from the experimental derivatives with those derived from the theory of reference 2. Although the phase angles derived from the experimental force and moment relations should agree, the difference between the two experimental curves is within the estimated accuracies of the derivatives. In view of the previously cited accuracy of C_{Z_ψ}, ±25 percent, the phase angles derived from the moment relations are considered more nearly accurate.

The flutter calculations of this report are based on the total moment derivatives:

$$C_{m_\theta}^* = C_{m_\theta} - \frac{l}{2R} C_{z_\theta}$$

$$C_{m_\psi}^* = -C_{n_\theta}^* = C_{m_\psi} - \frac{l}{2R} C_{z_\psi}$$

These experimental total moment coefficients are shown in figure 11. The estimated accuracies for these quantities are ± 5 percent for $C_{m_\theta}^*$ and ± 10 percent for $C_{n_\theta}^*$.

Mach number effects.- The effect of Mach number on the total moment coefficients $C_{m_\theta}^*$ and $C_{n_\theta}^*$ for $\beta_{0.75R} = 58°$ is shown in figure 13. Little effect is indicated for $C_{m_\theta}^*$, but $C_{n_\theta}^*$ appears to decrease with increasing Mach number. In contrast, theory would predict an increase in these derivatives given approximately by the Prandtl-Glauert correction factor $\dfrac{1}{\sqrt{1 - M^2}}$ at the lower Mach numbers.

Propeller Whirl Flutter

Whirl-flutter speeds.- In figure 14 the experimental whirl-flutter data for $l_0/R = 0.346$ are compared with theoretical boundaries for five blade angles. The data are presented in the form of damping required for stability as a function of reduced velocity $V/R\overline{\omega}$, the stable region being above the boundary. Since the air density varied somewhat from one test point to another (table II), the stability boundaries in figure 14 have been adjusted to represent a reference density value ρ_0 of 0.0022 slug/cu ft. As shown in appendix B, the appropriate density correction factor is ρ_0/ρ. Also, an average value of damping in the pitch and yaw directions is taken to be the representative damping, as reference 2 indicates no effect of the ratio of pitch damping to yaw damping for a symmetrical system. Thus, the damping parameter plotted is

$$\bar{g} = \frac{g_\theta + g_\psi}{2} \frac{\rho_0}{\rho}$$

or

$$\bar{\zeta} = \frac{\zeta_\theta + \zeta_\psi}{2} \frac{\rho_0}{\rho}$$

As considerable scatter exists in the damping measurements, a faired curve was obtained by fitting all the data for $l_0/R = 0.346$ in the least-squares sense to determine the coefficients of the following expression:

$$2\bar{\zeta} = \left[(-226.9 + 3.105\beta_{0.75R})\frac{V}{R\bar{\omega}} + \left(123.2 - 1.594\beta_{0.75R}\right)\left(\frac{V}{R\bar{\omega}}\right)^2\right]10^{-4}$$

This particular form can be justified as follows: The approximate whirl equation (eq. (26) of ref. 2) indicates that the theoretical whirl boundary may be approximated very closely by a parabola in $V/R\bar{\omega}$. A plot of the coefficients of this equation (eq. (26) of ref. 2) shows that they vary in a nearly linear manner with blade angle.

Figure 15 presents a comparison of the experimental and theoretical whirl-flutter boundaries for $l_0/R = 0.691$. Since all the measurements were made at approximately the same value of damping, $2\bar{\zeta} = 0.0059$ is taken as an average value and the data are presented in the form of reduced flutter speed $V/R\bar{\omega}$ as a function of blade angle. The stable region is below the curves. Observation of the data suggested the use of a parabola to fit the data. Therefore, the faired curve in this case was obtained by fitting the data in the least-squares sense to determine the coefficients of the parabola:

$$\frac{V}{R\bar{\omega}} = \left(3,054 - 6.61\beta_{0.75R} + 0.5243\beta_{0.75R}^2\right)10^{-3}$$

Theoretical flutter calculations would predict a curve of more complicated shape, but this approximation was considered satisfactory for the limited amount of data available.

Theoretical whirl boundaries were calculated by using equations (B6) and (B8). Since the nature of the damping in the system is unknown, calculations were made with the assumption of either viscous or structural damping. In these calculations the measured static-stability derivatives and C_{m_q} calculated by the method of reference 5 were used. For this system with $l_0/R = 0.346$ (fig. 14) and $l_0/R = 0.691$ (fig. 15) the use of viscous damping gives better agreement with experiment in that the errors are generally smaller and the shapes of the experimental and theoretical curves are more nearly the same. The agreement between the theoretical and experimental curves with viscous damping is excellent for $l_0/R = 0.346$, the largest error in reduced flutter speed being 6 percent. The error in speed for $l_0/R = 0.691$ is generally less than 10 percent.

Although the use of viscous damping in the calculations provides better agreement with measured whirl speeds in this case, such a result may not be true in general, particularly for aircraft structures.

Figures 16 and 17 show a comparison of experimental and theoretical (eqs. (B6) and (B8)) whirl boundaries for the measured static-stability derivatives (with the C_{m_q} of ref. 5), the derivatives of reference 5, and the derivatives of reference 3. Viscous damping is assumed. It is seen that the use of measured derivatives provides the best agreement. The calculated derivatives of

reference 5 provide better agreement than those of reference 3. The use of theoretical derivatives is conservative in that lower whirl speeds are predicted than were measured.

Figure 18 gives a comparison of the theoretical whirl speeds for $l_0/R = 0.346$ and $l_0/R = 0.691$ for three blade angles. It is seen that increasing l_0/R leads to a more stable system (higher flutter speed), as was indicated by references 2 to 4.

C_{m_q} required to predict whirl-flutter speeds.- Since no experimental values were available, it was of interest to determine the C_{m_q} required to predict the measured whirl speeds. This was done by using the measured system properties of inertia and viscous damping coefficient with the measured whirl speeds and measured static derivatives in equations (B6) and (B8) to solve for C_{m_q}. Ideally, this might also be considered the C_{m_q} inferred from the whirl-flutter speeds, but such a procedure should be considered to yield only an estimate in this case. The values of C_{m_q} computed for two values of damping when $l_0/R = 0.346$ and for the single value of damping when $l_0/R = 0.691$ are compared with theoretical values in figure 19. The inferred values of C_{m_q} for the three cases considered are in good agreement except for the data for $l_0/R = 0.691$ at the higher blade angles. The deviation of these points can possibly be attributed to the sensitivity of the whirl speeds to restraint damping, as indicated by the small slope for the higher blade angles at $l_0/R = 0.691$ in figure 18. The inferred values of C_{m_q} (fig. 19) exhibit the same trends as the theoretical values and are in good agreement with the values of reference 5 over most of the blade-angle range.

Whirl frequencies.- Figure 20 gives a comparison of experimental and theoretical whirl frequency ratios for $l_0/R = 0.346$ and for $l_0/R = 0.691$. The theory is shown to three degrees of approximation: first, including first-order aerodynamic terms (eq. (B6)); second, neglecting aerodynamic terms $\left(C_{m_\theta}^* = 0 \right.$ in eqs. (B7)$\left. \right)$; and third, neglecting aerodynamic terms and assuming the angular-momentum ratio $\frac{I_X \Omega}{I_Y \omega} \ll 1$ (eq. (B10)). It is seen that the calculations in which $C_{m_\theta}^*$ is retained provide the best overall agreement, the largest error being 8 percent.

Wing effects.- Some tests were made in which the nacelle-engine-propeller model treated in this paper was mounted on a semispan wing cantilevered from the tunnel wall as previously discussed in the section entitled "Models." Whirl-flutter speeds for two levels of damping are presented in figure 21, and are compared with results from the tests of the isolated model. This comparison indicates that the wing had little effect on the whirl speeds. Whirl frequencies ranged from 5.7 cps to 8.9 cps.

The question of the effects of the wing is a broad problem, and therefore the small effect illustrated in figure 21 may not be typical of the results for other configurations. It should also be noted that in the experimental results presented in reference 2 for a four-engine model, the presence of a wing and complete model have large effects (up to 100 percent).

CONCLUSIONS

A wind-tunnel investigation of propeller whirl flutter was made with an isolated combination of a windmilling propeller and simulated power plant over a range of propeller blade angles, restraint stiffnesses, and restraint damping coefficients for a system symmetrical in pitch and yaw. Measurements of the static-stability derivatives of the windmilling propeller were also made with a simple balance. Limited whirl-flutter results were obtained for the model mounted on a cantilever wing. The following conclusions are indicated:

1. The measured whirl-flutter speeds and frequencies for the isolated model were in very good agreement with those predicted by calculations in which measured static derivatives and viscous damping were used. This agreement was better than that obtained using structural damping.

2. Predicted whirl-flutter speeds for the isolated model were lower when theoretical stability derivatives were used than when measured static derivatives were used.

3. Theoretical static-stability derivatives obtained by two methods exhibited the same trends as experimental derivatives, but differed appreciably in magnitude in certain instances. Limited measurements at one blade angle indicated that Mach number had little effect.

4. Little effect of the wing on the measured whirl-flutter boundaries was indicated by the limited data available for the one configuration considered, although previous investigations have shown larger effects of the wing.

Langley Research Center,
    National Aeronautics and Space Administration,
        Langley Station, Hampton, Va., April 8, 1963.

DATA REDUCTION FOR STATIC-DERIVATIVE MEASUREMENTS

Determination of C_{m_θ} and C_{Z_θ}

The static equation governing the pitch deflection of the engine-propeller system may be obtained from equation (B1). The result is

$$k^2\theta = \kappa\left(C^*_{m_\theta}\theta + C^*_{m_\psi}\psi\right) \tag{A1}$$

For measurement of $C^*_{m_\theta}$ the gimbal was arranged to allow pitch freedom only. Hence, for $\psi = 0$, the pitching-moment coefficient is

$$C^*_m = \frac{K_\theta\theta}{qSD} \tag{A2}$$

where $K_\theta\theta$ is the moment measured by the strain gage. The experimental data are presented in figures 22 and 23, where the moment coefficient C^*_m is plotted against the measured pitch angle θ. The slope of these curves is $C^*_{m_\theta}$.

Two distances between the gimbal axis and propeller plane were used in order to separate the force and moment contributions to the total moment. The equations are

$$\left.\begin{aligned}
C^*_{m_\theta,1} &= C_{m_\theta} - \frac{l_1}{2R} C_{Z_\theta} \\
C^*_{m_\theta,2} &= C_{m_\theta} - \frac{l_2}{2R} C_{Z_\theta}
\end{aligned}\right\} \tag{A3}$$

where the subscripts 1 and 2 refer to data for $l_o/R = 0.346$ and $l_o/R = 0.691$, respectively. Equations (A3) are solved to give

$$C_{m_\theta} = \frac{1}{l_2 - l_1}\left(l_2 C^*_{m_\theta,1} - l_1 C^*_{m_\theta,2}\right) \tag{A4}$$

$$C_{Z_\theta} = \frac{2R}{l_2 - l_1}\left(C^*_{m_\theta,1} - C^*_{m_\theta,2}\right) \tag{A5}$$

The quantities $c_{m_\theta,1}^*$ and $c_{m_\theta,2}^*$ from which C_{m_θ} and C_{Z_θ} are derived are given in figure 11. Figure 10 shows the variation of C_{m_θ} and C_{Z_θ} with blade angle.

<center>Determination of C_{m_ψ} and C_{Z_ψ}</center>

The static equation governing the yaw deflection of the engine-propeller system may also be obtained from equation (B1) by letting $c_{m_\theta}^* = c_{n_\psi}^*$ and $c_{m_\psi}^* = -c_{n_\theta}^*$. The result is

$$k^2 \psi = \kappa \left(c_{n_\psi}^* \psi + c_{n_\theta}^* \theta \right) \tag{A6}$$

For the determination of $c_{n_\theta}^*$ the gimbal was allowed yaw freedom only. The yawing-moment coefficient is found to be

$$c_n^{**} = \frac{K_\psi \psi}{qSD} = c_{n_\psi}^* \psi + c_{n_\theta}^* \theta \tag{A7}$$

where $K_\psi \psi$ is the moment measured by the strain gage. The experimental data are presented in figures 22 and 23. The slopes of these curves $\left(c_{n_\theta}^{**} \right)$ are used to obtain $c_{n_\theta}^*$ by applying equation (A7); that is,

$$c_{n_\theta}^* = c_{n_\theta}^{**} - c_{n_\psi}^* \frac{\psi}{\theta} \tag{A8}$$

The ratio ψ/θ is a constant for a given blade angle and dynamic pressure, and was obtained by plotting ψ (as determined from strain-gage output) against θ (as determined from the sting angle of attack). Since ψ/θ depends on dynamic pressure, c_n^{**} does also, as shown in figures 22 and 23. The relation $c_{n_\psi}^* = c_{m_\theta}^*$ was used to obtain $c_{n_\psi}^*$.

By using $c_{n_\theta}^* = -c_{m_\psi}^*$, the resolution of $c_{m_\psi}^*$ into its components is carried out in the same manner as that for $c_{m_\theta}^*$ (see eqs. (A3)). The results are

$$C_{m_\psi} = \frac{1}{l_2 - l_1} \left(l_1 c_{n_\theta,2}^* - l_2 c_{n_\theta,1}^* \right) \tag{A9}$$

$$C_{Z_\psi} = \frac{2R}{l_2 - l_1} \left(c_{n_\theta,2}^* - c_{n_\theta,1}^* \right) \tag{A10}$$

16

The quantities $C^*_{n_\theta,1}$ and $C^*_{n_\theta,2}$ from which C_{m_ψ} and C_{Z_ψ} are derived are given in figure 11. Figure 10 shows the variation of C_{m_ψ} and C_{Z_ψ} with blade angle.

APPENDIX B

EQUATIONS OF MOTION

The equations of motion for a two-degree-of-freedom engine-propeller system disturbed from equilibrium are derived in reference 2. With some changes in notation, the equations for a system symmetrical in pitch and yaw are (omitting the aerodynamic acceleration terms)

$$\left. \begin{aligned} \theta'' + \frac{H}{J}\psi' + g\frac{k}{\lambda}\theta' + k^2\theta &= \kappa\left(C_{m_\theta}^*\theta + C_{m_q}^*\theta' + C_{m_\psi}^*\psi + C_{m_r}^*\psi'\right) \\ \psi'' - \frac{H}{J}\theta' + g\frac{k}{\lambda}\psi' + k^2\psi &= \kappa\left(C_{m_\theta}^*\psi + C_{m_q}^*\psi' - C_{m_\psi}^*\theta - C_{m_r}^*\theta'\right) \end{aligned} \right\} \quad \text{(B1}$$

The propeller aerodynamic derivatives are

Total pitching-moment derivative due to pitch angle:

$$C_{m_\theta}^* = C_{m_\theta} - \frac{l}{2R}C_{Z_\theta} \quad \text{(B2}$$

Total pitching-moment derivative due to yaw angle:

$$C_{m_\psi}^* = C_{m_\psi} - \frac{l}{2R}C_{Z_\psi} \quad \text{(B3}$$

Total pitching-moment derivative due to pitch rate:

$$C_{m_q}^* = C_{m_q} - \frac{l}{2R}C_{Z_q} - \frac{l}{R}C_{m_\theta}^* \quad \text{(B4}$$

Total pitching-moment derivative due to yaw rate:

$$C_{m_r}^* = C_{m_r} - \frac{l}{2R}C_{Z_r} - \frac{l}{R}C_{m_\psi}^* \quad \text{(B5}$$

For the present purpose, C_{Z_q} and $C_{m_r}^*$, which are considered small in this case will be neglected. The derivative C_{m_θ}, which was neglected in reference 2, is included here.

The assumption of a harmonic time dependence leads to the characteristic equation for neutral stability. The real part yields the whirl frequency equation

$$\lambda^2 = P - \sqrt{P^2 - Q} \tag{B6}$$

where

$$P = 1 + \left[\frac{1}{2}\left(\frac{H}{J}\right)^2 - \kappa C_{m_\theta}^*\right]\left(\frac{1}{k}\right)^2$$

$$Q = 1 - 2\kappa C_{m_\theta}^*\left(\frac{1}{k}\right)^2 \tag{B7}$$

Terms involving products of aerodynamic and damping terms are small and are therefore neglected. The imaginary part of the characteristic equation gives the viscous damping required for neutral stability:

$$2\zeta = \kappa \frac{1}{k}\left[C_{m_q}^* + \frac{\frac{H}{J}C_{m_\psi}^*\left(\frac{1}{k}\right)^2}{1 - \lambda^2 - \kappa C_{m_\theta}^*\left(\frac{1}{k}\right)^2}\right] \tag{B8}$$

The structural damping required for stability is (from ref. 2)

$$g = 2\zeta\lambda \tag{B9}$$

An approximate expression for the frequency is obtained by assuming

$$\frac{H}{J}\frac{1}{k} = \frac{I_X\Omega}{I_Y\overline{\omega}} \ll 1$$

The result is (from ref. 2)

$$\lambda = 1 - \frac{H}{2Jk} \tag{B10}$$

Since κ is proportional to ρ, and $\kappa C_{m_\theta}^*\left(\frac{1}{k}\right)^2$ is small in comparison with $1 - \lambda^2$, equation (B8) indicates that $2\zeta/\rho$ should be approximately independent of the air density. This result was used to adjust the experimental whirl data for the small variations in density. The values of damping coefficient ($\overline{g}$ or 2ζ) plotted were obtained by multiplying the average measured coefficients by ρ_0/ρ.

REFERENCES

1. Taylor, E. S., and Browne, K. A.: Vibration Isolation of Aircraft Power Plants. Jour. Aero. Sci., vol. 6, no. 2, Dec. 1938, pp. 43-49.

2. Reed, Wilmer H., III, and Bland, Samuel R.: An Analytical Treatment of Aircraft Propeller Precession Instability. NASA TN D-659, 1961.

3. Houbolt, John C., and Reed, Wilmer H., III: Propeller-Nacelle Whirl Flutter. Jour Aerospace Sci., vol. 29, no. 3, Mar. 1962, pp. 333-346.

4. Sewall, John L.: An Analytical Trend Study of Propeller Whirl Instability. NASA TN D-996, 1962.

5. Ribner, Herbert S.: Propellers in Yaw. NACA Rep. 820, 1945. (Supersedes NACA ARR 3L09.)

6. Abbott, Frank T., Jr., Kelly, H. Neale, and Hampton, Kenneth D.: Investigation of Propeller—Power-Plant Autoprecession Boundaries for a Dynamic-Aeroelastic Model of a Four-Engine Turboprop Transport Airplane. NASA TN D-1806, 1963.

7. McLemore, H. Clyde, and Cannon, Michael D.: Aerodynamic Investigation of a Four-Blade Propeller Operating Through an Angle-of-Attack Range From 0° to 180°. NACA TN 3228, 1954.

TABLE I.- SUMMARY OF MODEL CHARACTERISTICS

I_X, slug-ft^2 . . . . 0.00858

I_Y (for $l_o/R = 0.346$), slug-ft^2 . . . . 0.0634

I_Y (for $l_o/R = 0.691$), slug-ft^2 . . . . 0.0937

R, ft 0.8438

$b_{0.75R}$, ft 0.1823

σ 0.1834

TABLE II.- MODEL TEST DATA

(a) Sting-mounted configurations with $l_o/R = 0.346$

$\beta_{0.75R}$, deg	f_θ, cps	f_ψ, cps	$2\zeta_\theta$	$2\zeta_\psi$	ρ, slugs/cu ft	n, rps	V_f, ft/sec	f_f, cps
35	9.20	9.12	0.0060	0.0090	0.00211	38.4	120	6.88
46	↓	↓	↓	↓	.00210	26.2	118	7.37
52				.0163	↓	22.0	122	7.63
58	↓	↓	↓	.0126	↓	19.4	139	7.73
25	9.71	9.65	.0058	.0131	.00210	60.0	125	6.20
46				↓	↓	28.8	131	7.80
52				.0076	↓	24.1	138	8.10
58	↓	↓	↓	.0098	.00211	20.0	144	8.20
25	10.43	10.26	.0066	.0216	↓	64.4	136	6.42
35			↓		.00210	40.2	128	7.60
46			.0060		↓	30.4	136	8.16
46			↓		↓	31.8	143	8.05
52	↓	↓	.0066	↓	.00209	26.1	148	8.39
35	10.96	10.96	.0150	.0238	.00217	51.8	159	7.58
46					.00218	37.3	167	8.30
52					.00209	33.0	186	8.63
58	↓	↓	↓	↓	↓	29.2	210	8.75
35	11.52	11.50	.0152	.0218	.00218	56.2	173	8.08
46					.00217	41.0	188	8.83
52					↓	35.4	202	8.98
58	↓	↓	↓	↓	.00216	30.1	222	9.27
25	10.44	10.40	.0153	.0263	.00218	72.1	152	6.26
33			↓	↓	↓	53.4	150	6.96
46			.0126	.0200	↓	36.0	161	8.13
52			↓		.00219	29.4	165	8.55
58	↓	↓	.0150	↓	↓	24.2	171	8.66
25	10.46	10.51	.0175	.0398	.00219	81.3	172	6.00
33				↓	.00220	58.7	163	6.62
46				.0316	↓	41.4	182	7.61
52				.0398	.00219	35.3	196	7.71
58	↓	↓	↓	.0368	↓	29.0	210	8.19
25	10.71	10.28	.0371	.0393	.00220	85.6	179	5.56
46			.0300			44.6	196	7.60
52			.0371			38.4	213	7.73
58	↓	↓	.0300	↓	↓	33.2	231	8.10

TABLE II.- MODEL TEST DATA - Concluded

(b) Sting-mounted configurations with $l_0/R = 0.691$

$\beta_{0.75R}$, deg	f_θ, cps	f_ψ, cps	$2\zeta_\theta$	$2\zeta_\psi$	ρ, slug/cu ft	n, rps	V_f, ft/sec	f_f, cps
25	7.60	7.60	0.0056	0.0053	0.00226	59.4	120	4.94
35	↓	↓	↓	↓	.00227	48.8	145	5.27
46					.00226	37.6	171	5.57
52					↓	31.0	172	5.66
$27\frac{1}{2}$	7.64	7.68	.0060	.0074	↓	63.2	144	4.73
35				↓	.00220	44.4	134	5.50
35				.0062	↓	46.8	141	5.39
$39\frac{1}{2}$				↓	.00226	40.3	140	5.78
46				.0074	.00220	33.2	147	5.81
52				.0062	.00221	28.4	156	6.00
58	↓	↓	↓	↓	.00220	26.3	183	6.09

(c) Wing-mounted configurations with $l_0/R = 0.346$

$\beta_{0.75R}$, deg	f_θ, cps	f_ψ, cps	$2\zeta_\theta$	$2\zeta_\psi$	ρ, slug/cu ft	n, rps	V_f, ft/sec	f_f, cps
25	9.21	9.34	0.0072	0.0132	0.00232	61.5	125	5.70
35	↓	↓	↓	↓	.00231	41.0	121	6.58
46					.00232	29.0	126	7.24
52					↓	25.0	135	7.40
58	↓	↓	↓	↓	.00231	21.5	148	7.67
35	11.6	11.7	.0290	.0324	↓	63.5	188	7.60
46					.00230	46.5	202	8.41
52					.00228	40.0	216	8.60
58	↓	↓	↓	↓	.00233	36.0	251	8.94
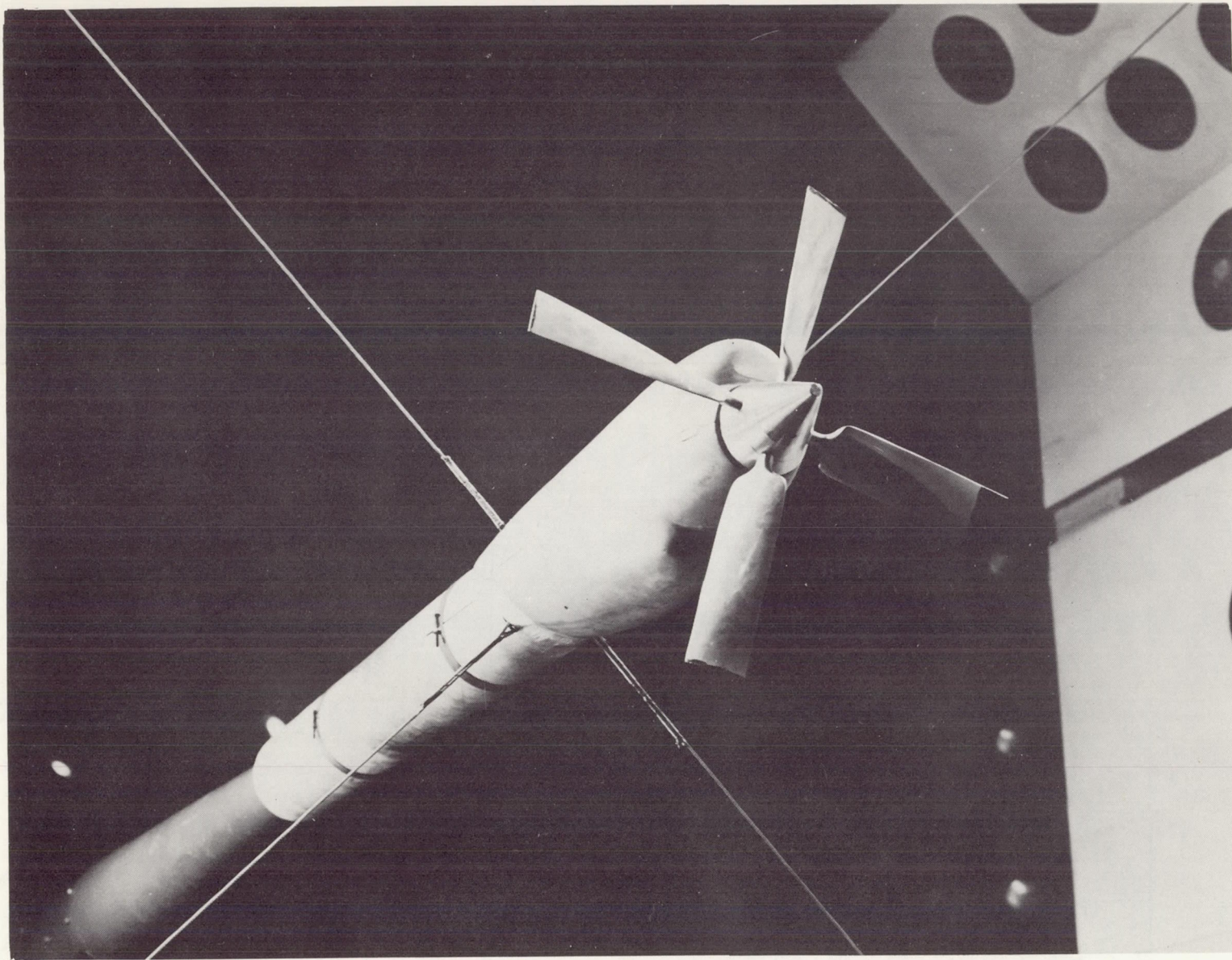
L-61-6611

Figure 1.- Photograph of sting-mounted propeller whirl model in the test section of the Langley transonic dynamics tunnel.

Propeller shaft   Shaft housing   Gimbal

INCHES
0   1   2
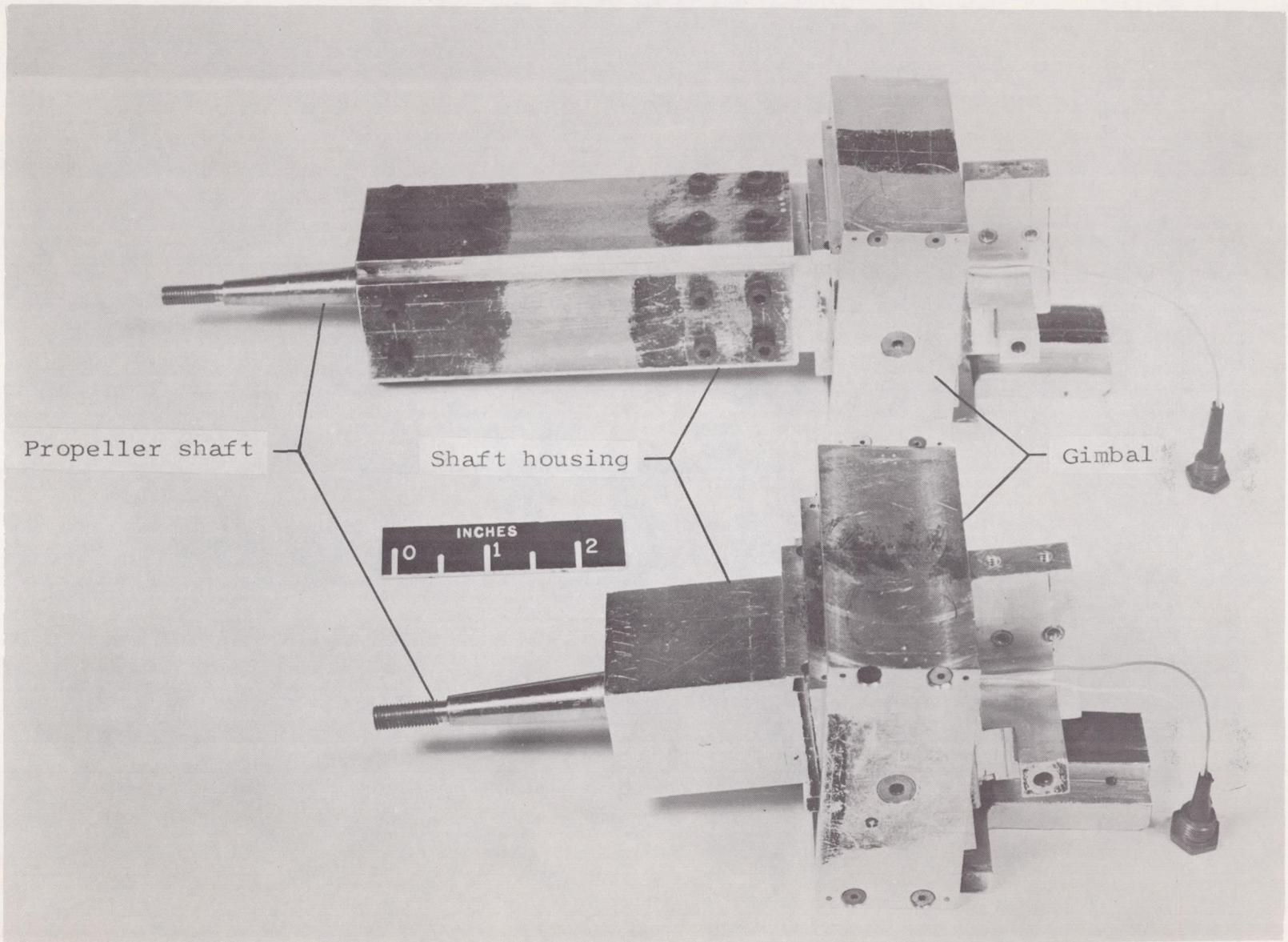
L-61-6610.1

Figure 2.- Photograph of gimbal with long shaft and of gimbal with short shaft.

26
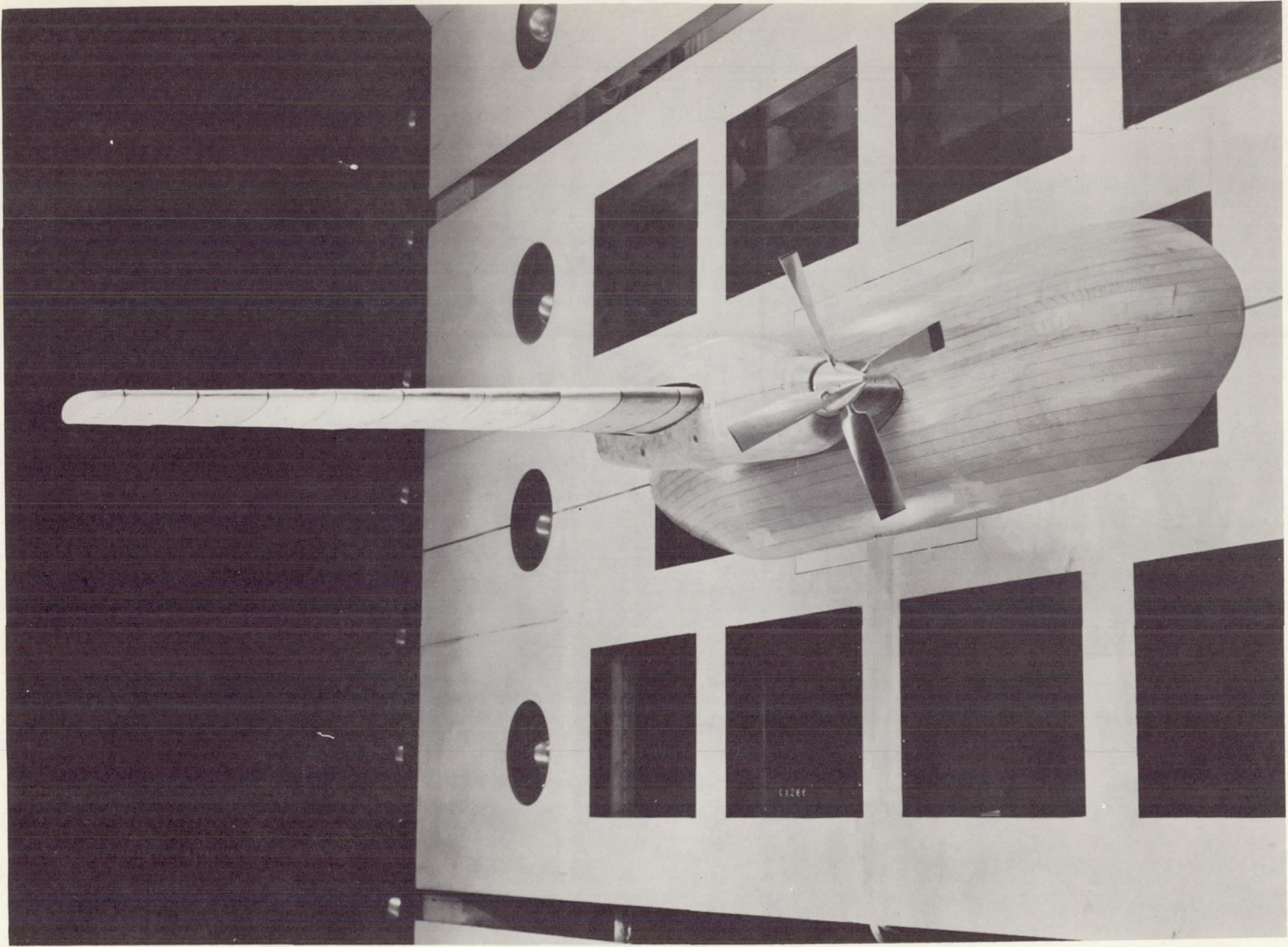
L-61-291

Figure 3.- Photograph of wing-mounted propeller whirl model in the test section of the Langley transonic dynamics tunnel.
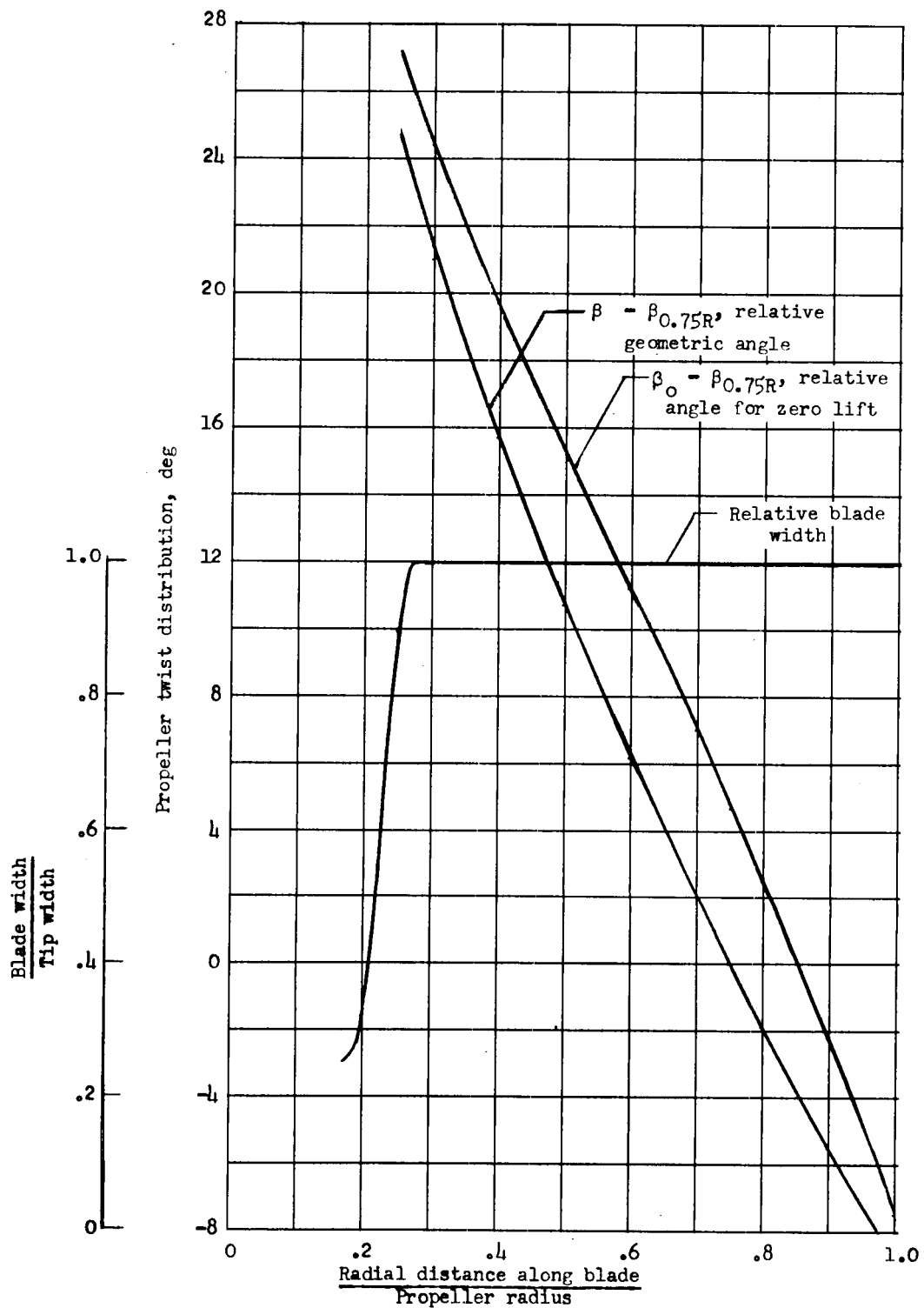
Figure 4.- Distribution of propeller twist angle and blade width for the airplane propeller of this analysis.
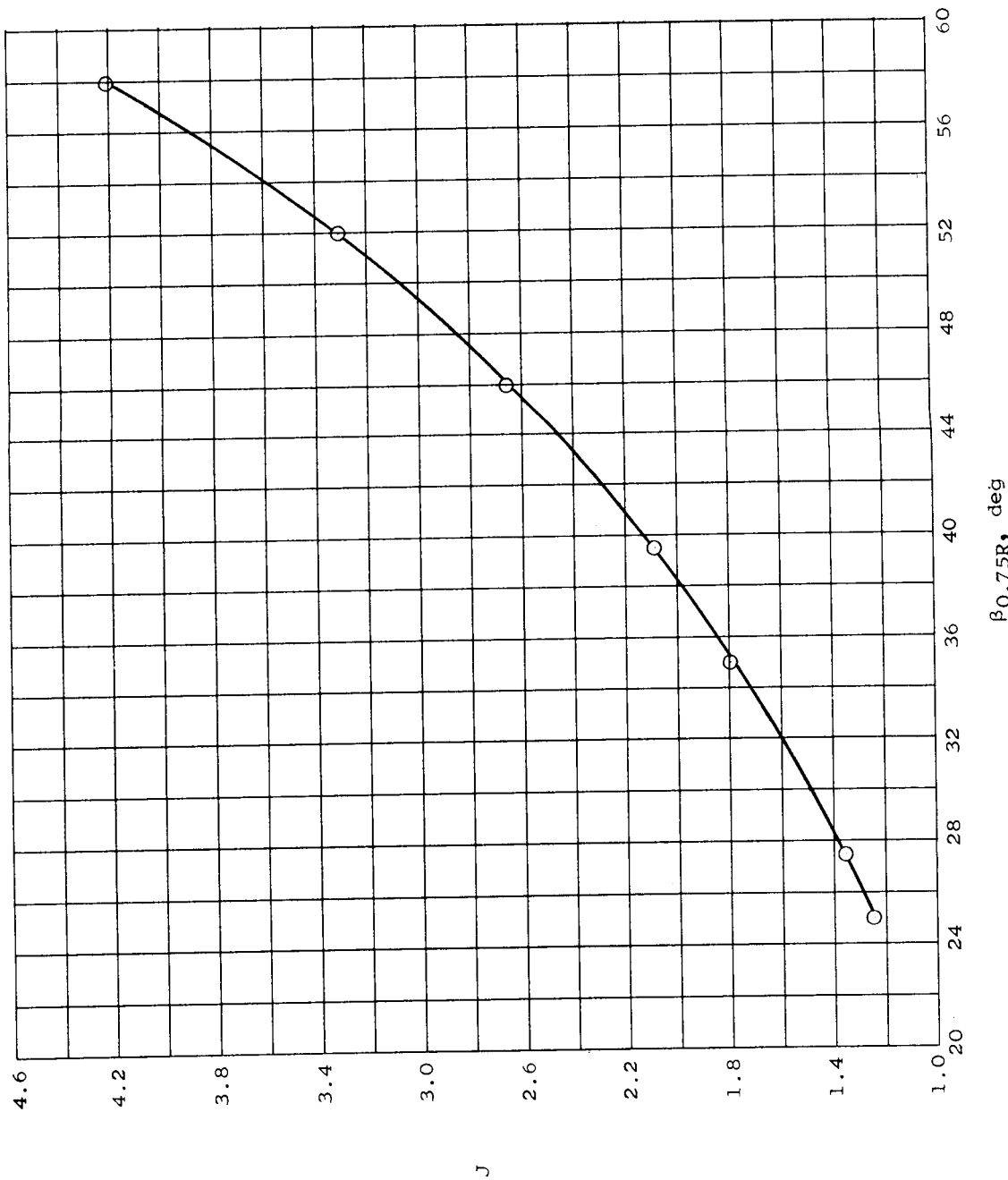
Figure 5.- Experimental variation of advance ratio with geometric blade angle at three-quarter-radius station for windmilling propeller.
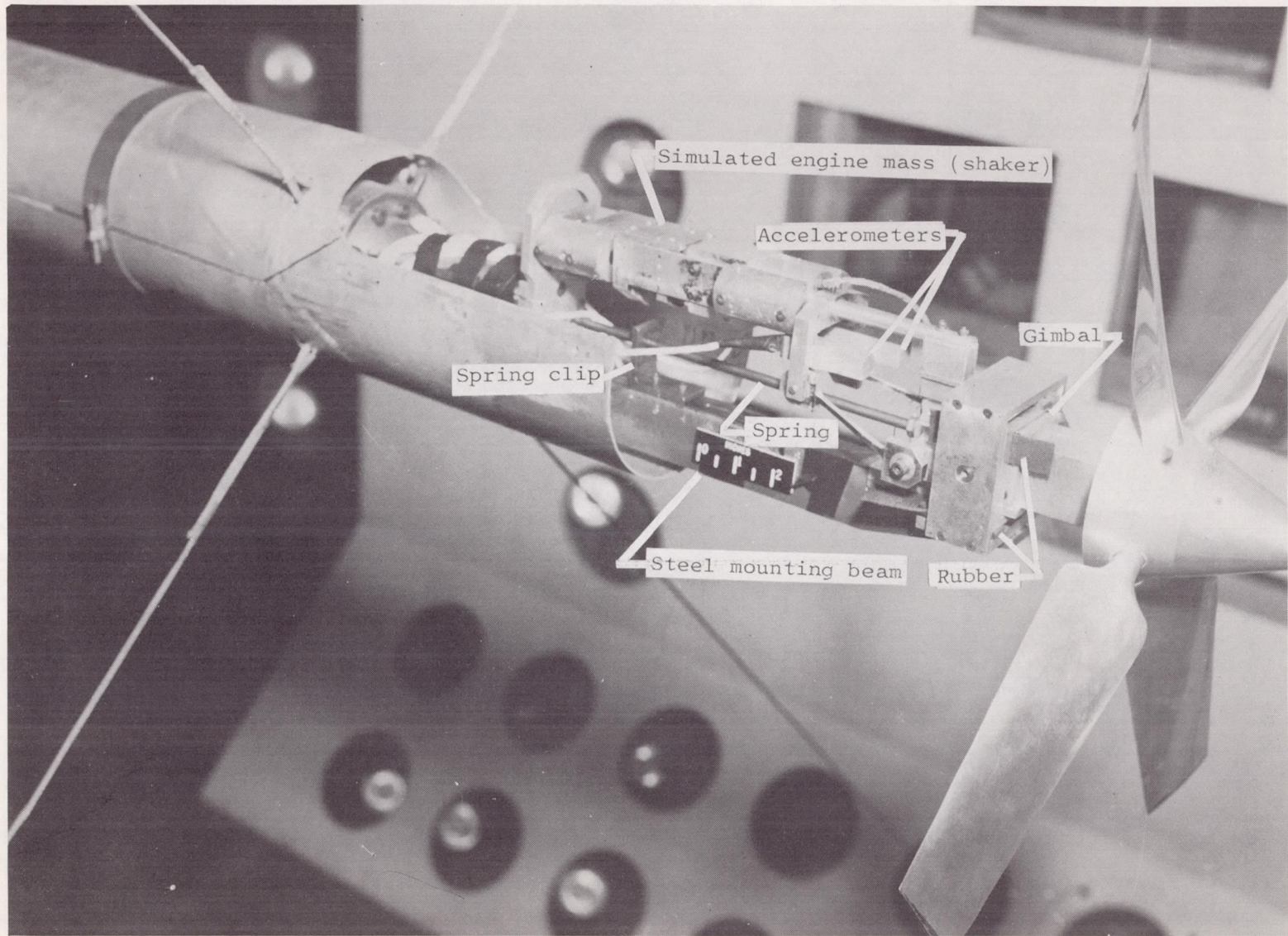
Figure 6.- Photograph of sting-mounted propeller whirl model showing details of design.   L-61-6614.1

Simulated engine mass (shaker)

Gimbal restraint spring
(fixed to shaft housing on
center line of shaft axis)

Yaw axis

Gimbal

Pitch axis

Shaft housing

Sting adapter

Propeller shaft

Alternate clip positions
for stiffness variations

Mounting beam
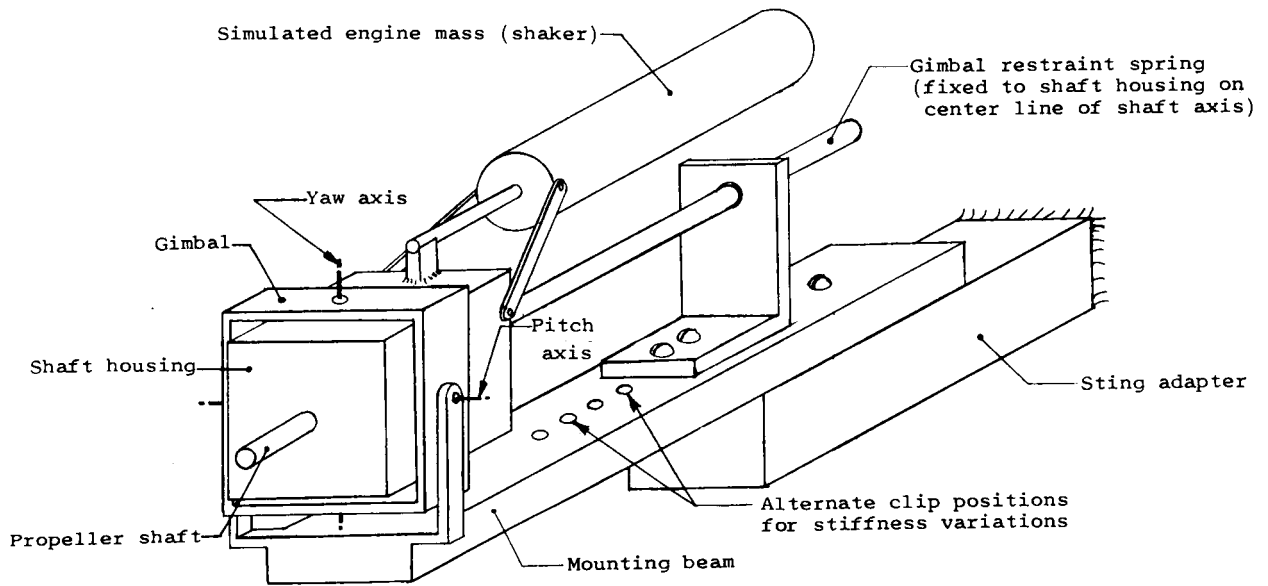
(a) Power plant, gimbal, and mounting for whirl-flutter model.

Simulated engine mass(shaker)

Mounting bolts

Pitch-angle
accelerometer

Gimbal with locked
yaw axis

Pitch axis

Shaft housing

Sting
adapter

Propeller shaft

Alternate position for
mounting bolts for yawing-
moment measurements

Flexible clip

Strain-gage beam

Mounting beam
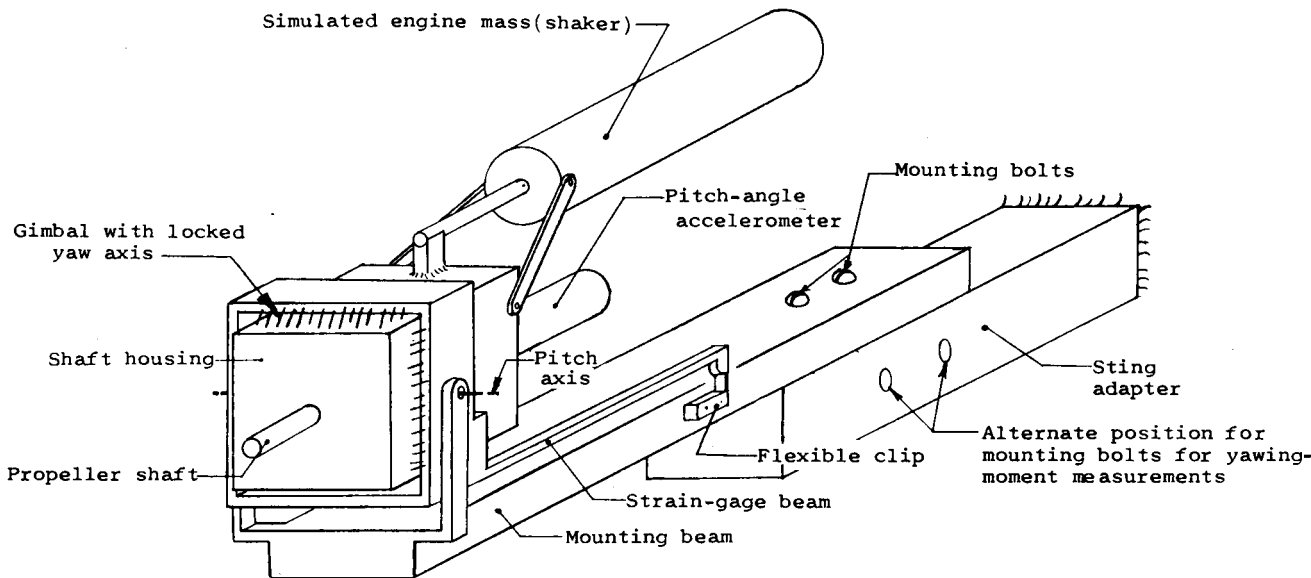
(b) Derivative-measurement model.

Figure 7.- Schematic drawings of isolated models.
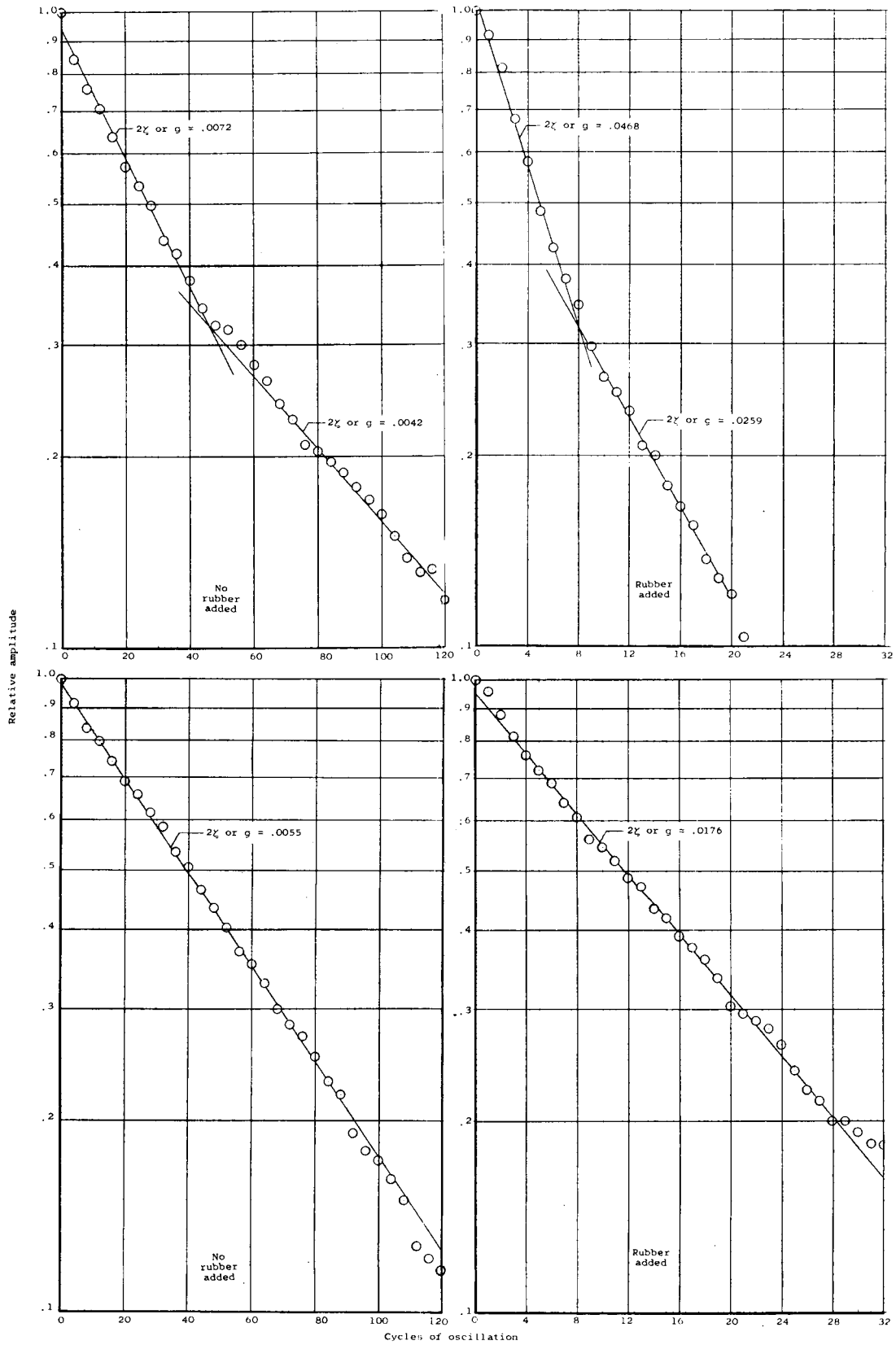
Figure 8.- Typical records of decay of free vibration.
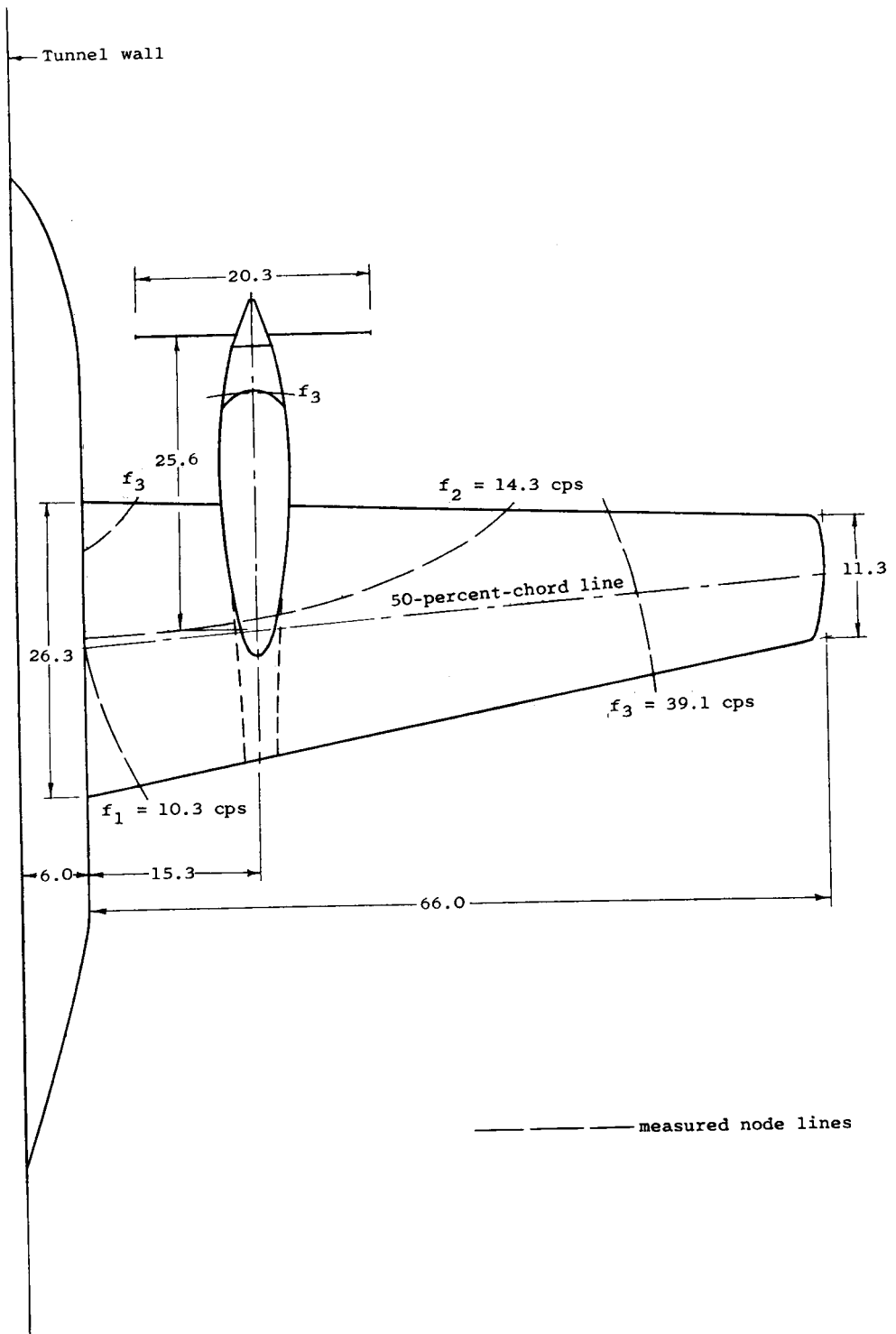
Figure 9.- Sketch of cantilever-wing model in tunnel, showing measured node lines and frequencies of the wing. All dimensions are in inches unless otherwise specified.
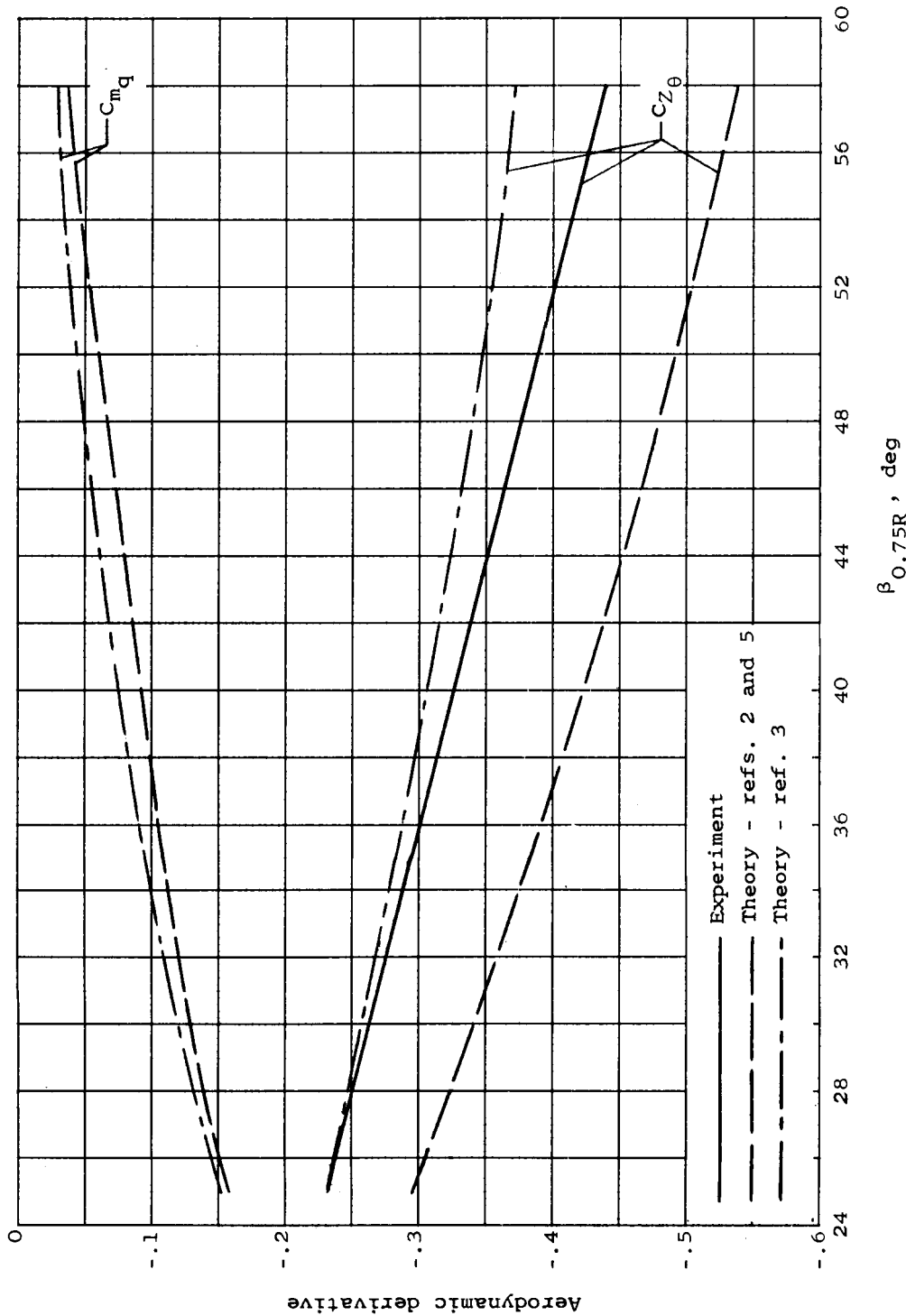
Figure 10.- Comparison of experimental and theoretical aerodynamic derivatives for propeller.

(a) C_{Z_θ} and C_{m_q}.

33

$\beta_{0.75R}$, deg

(b) $c_{m_{\dot{q}}}$.

Figure 10.- Continued.

Aerodynamic derivative

Experiment

Theory - refs. 2 and 5

Theory - ref. 3

(c) C_{Z_ψ} and C_{m_θ}.
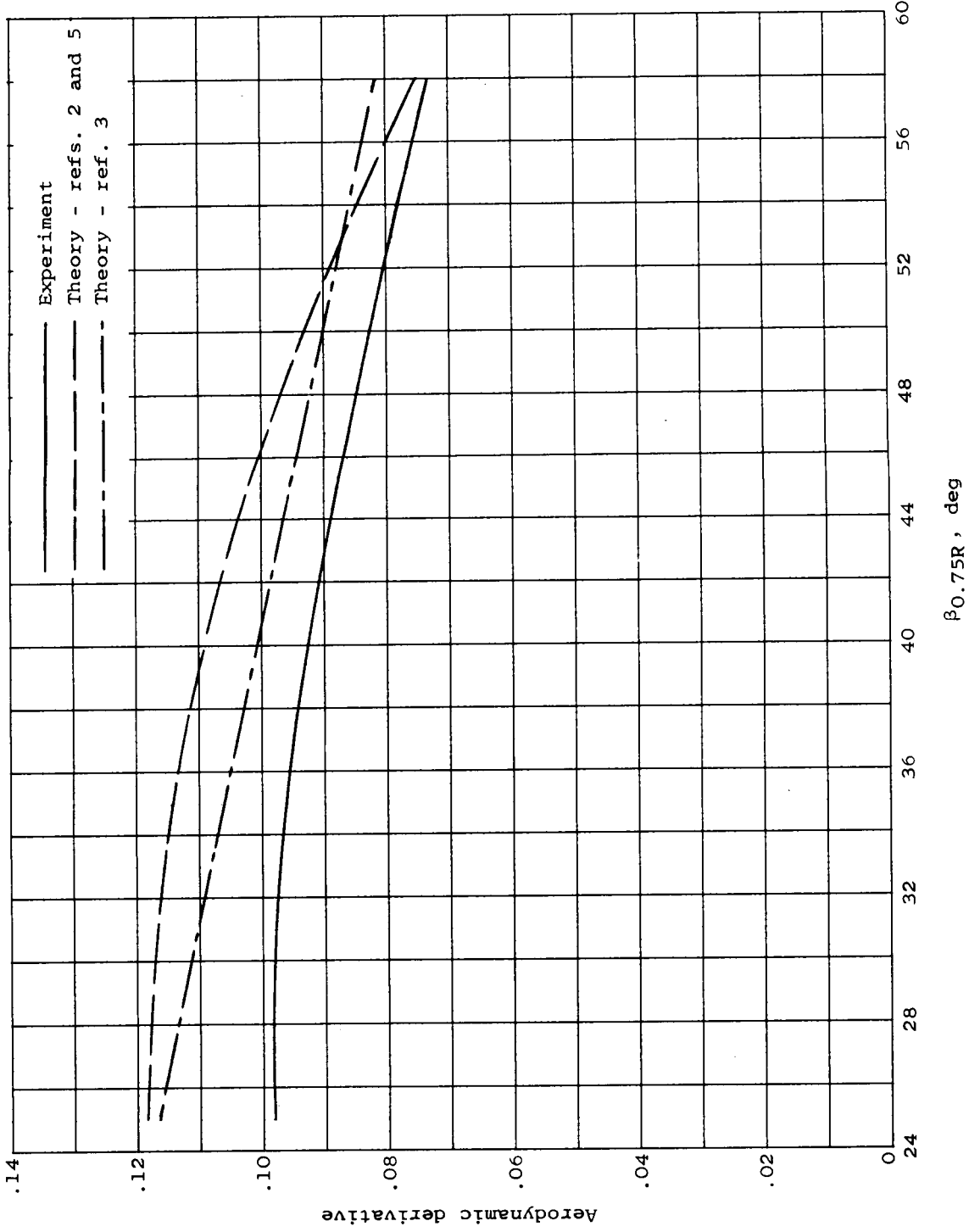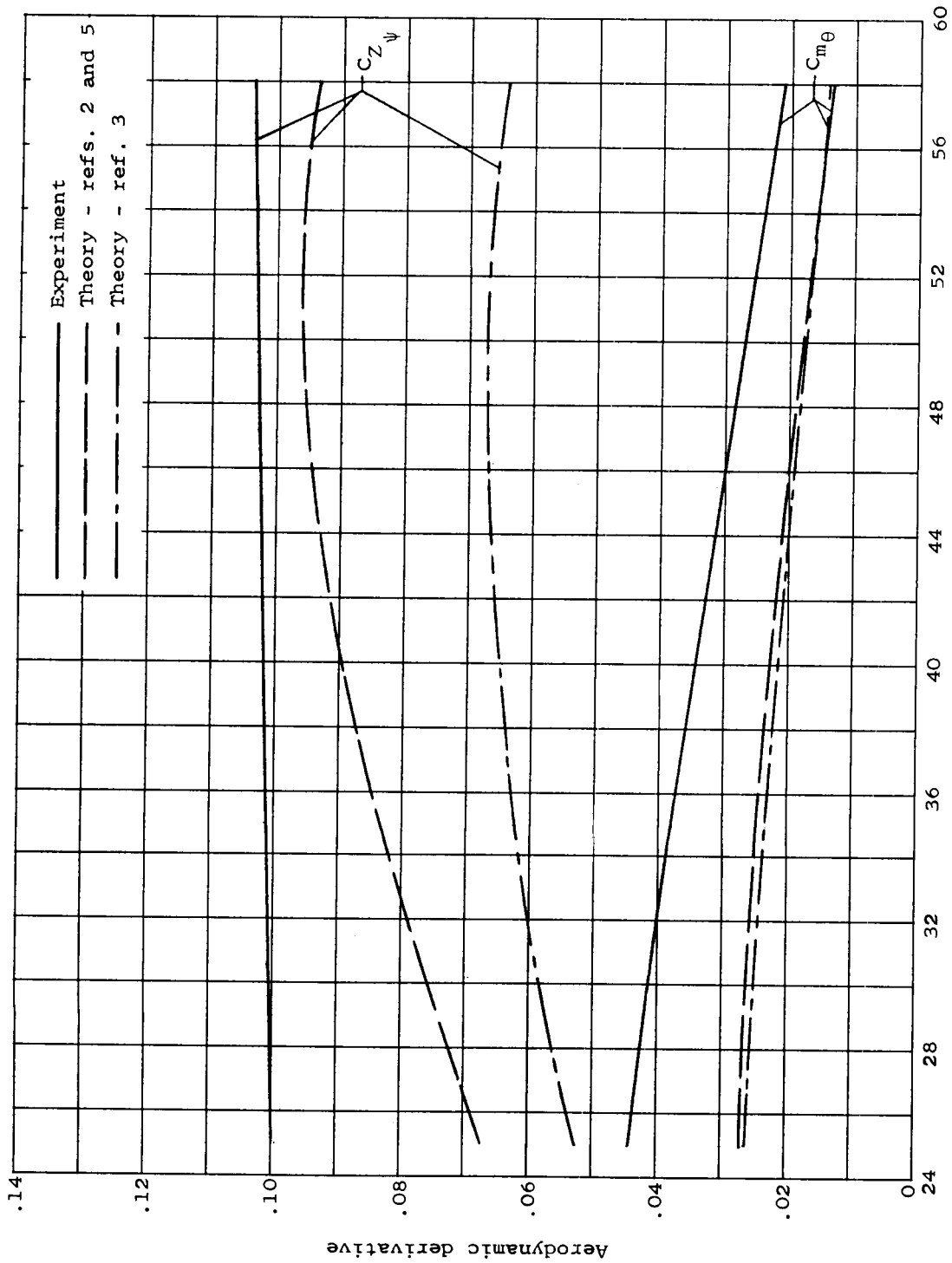
Figure 10.- Concluded.

35
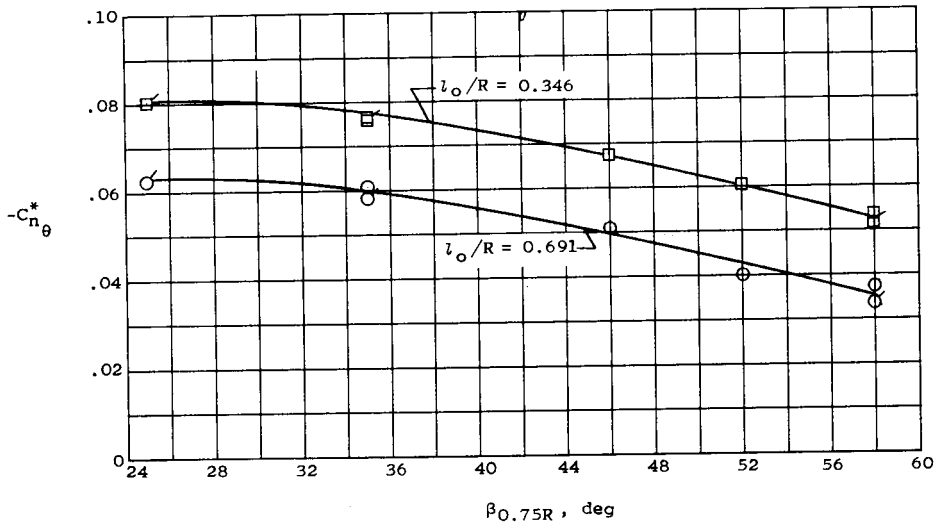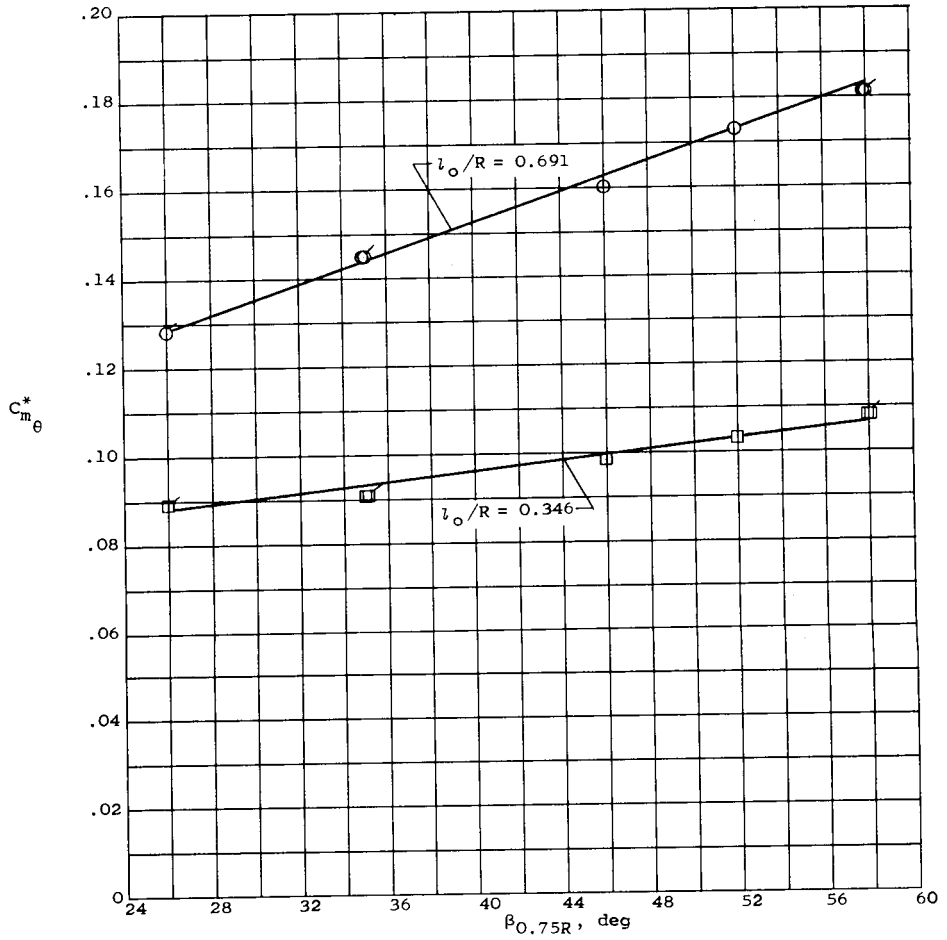
Figure 11.- Variation of $C_{m_\theta}^*$ and $C_{n_\theta}^*$ with propeller reference blade angle. Plain symbols indicate data taken at a dynamic pressure of 100 lb/sq ft; flagged symbols, 50 lb/sq ft.
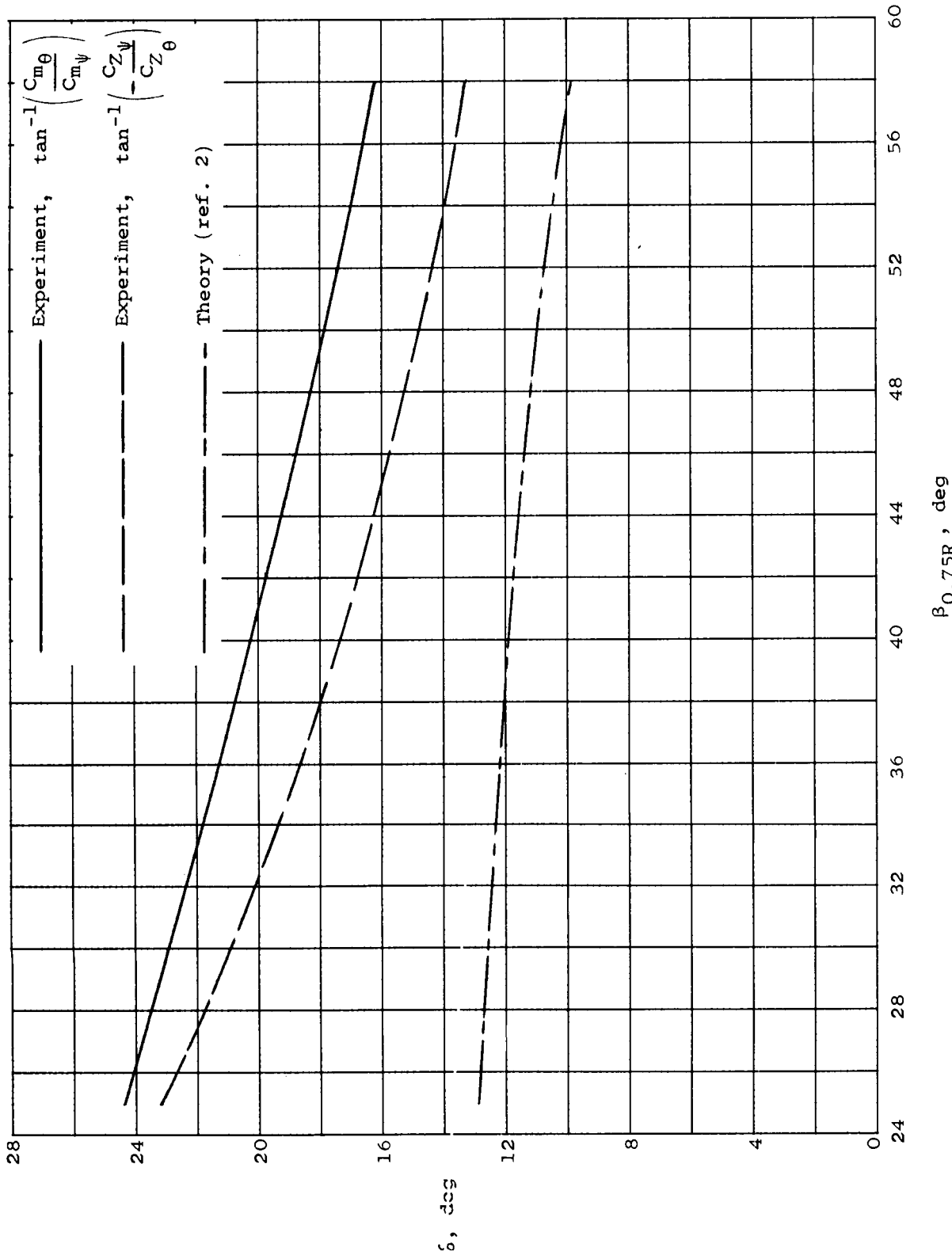
Figure 12.- Comparison of experimental and theoretical lift-lag phase angle.
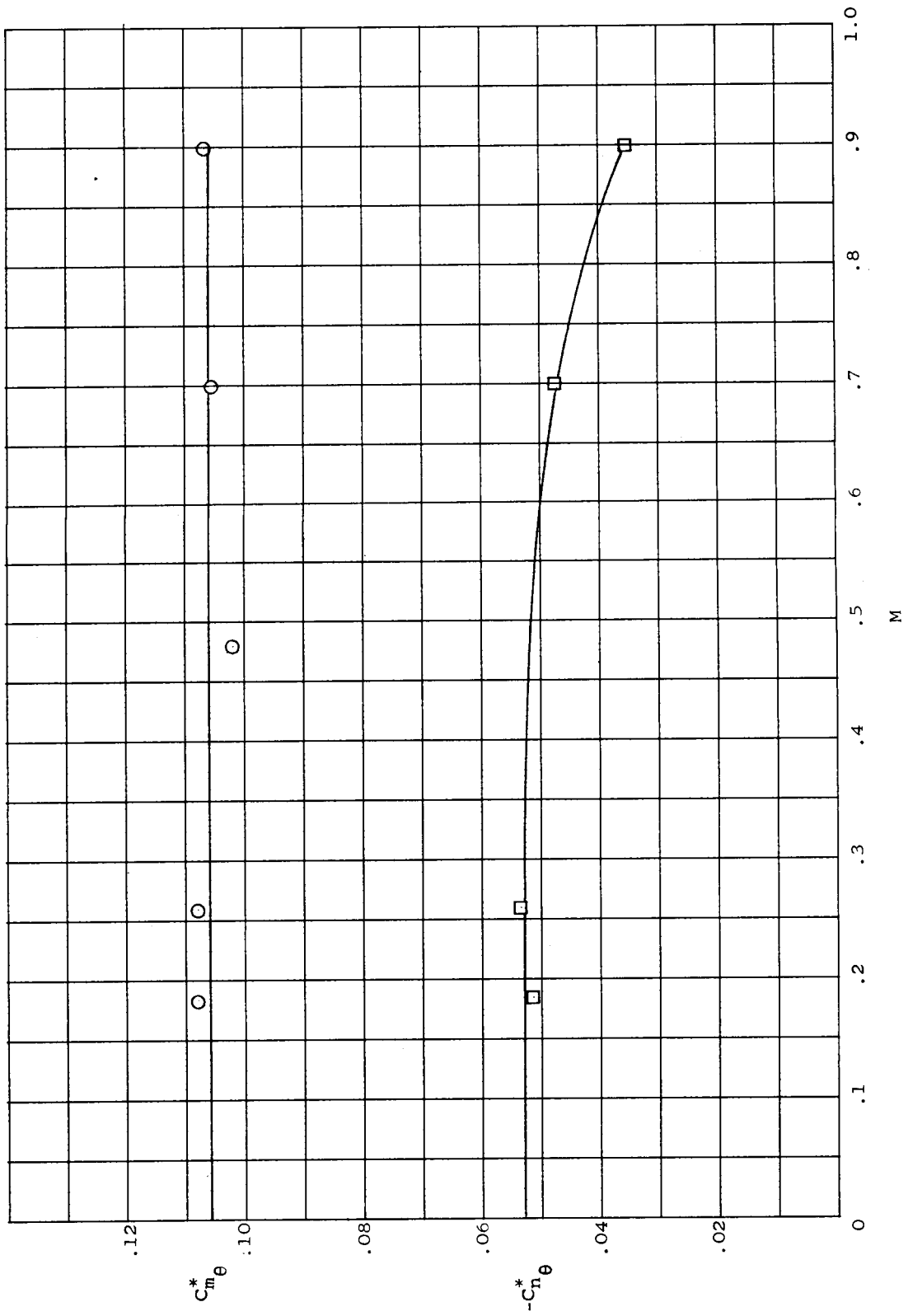
Figure 13.- Variation of $C_{m_\theta}^*$ and $C_{n_\theta}^*$ with Mach number. $\beta_{0.75R} = 58^\circ$.
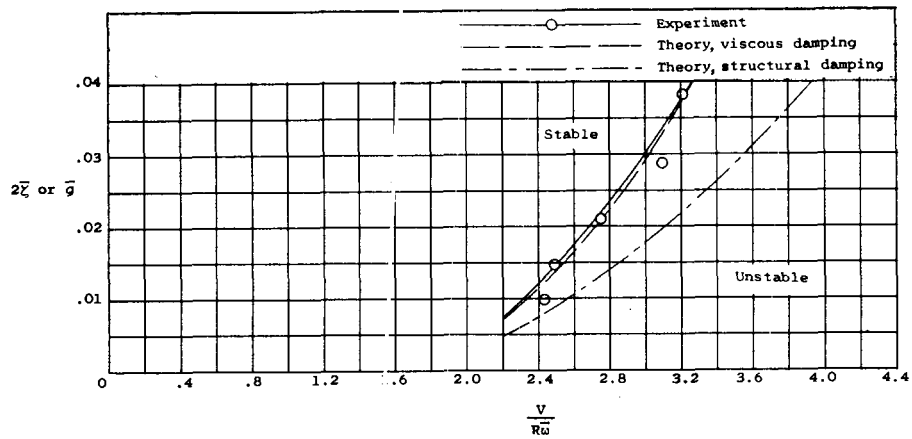
(a) $\beta_{0.75R} = 25^{\circ}$.
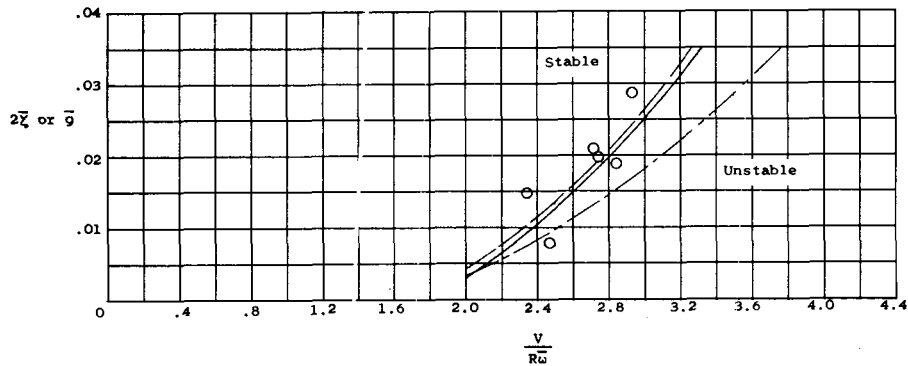
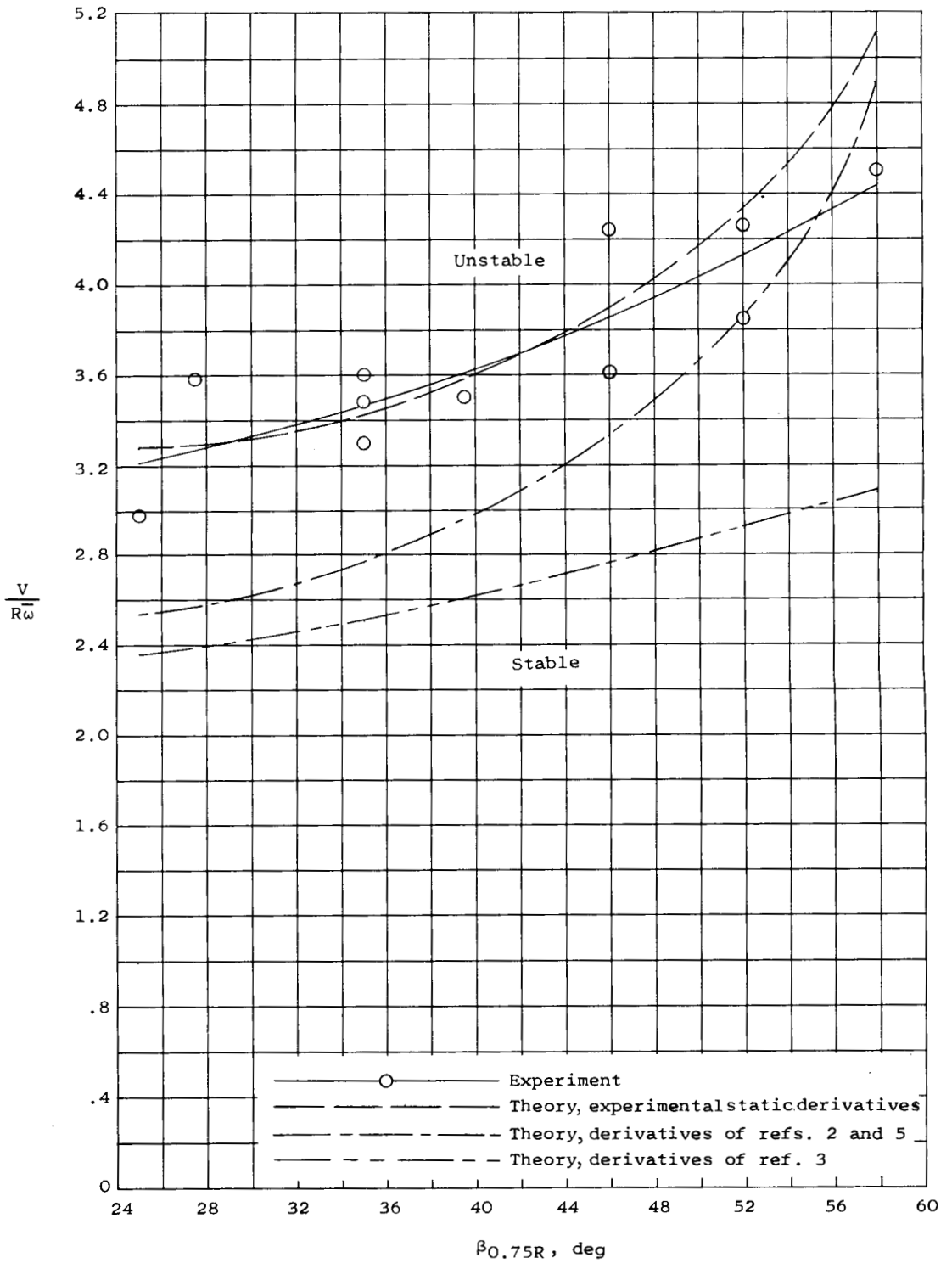(b) $\beta_{0.75R} = 35^{\circ}$.
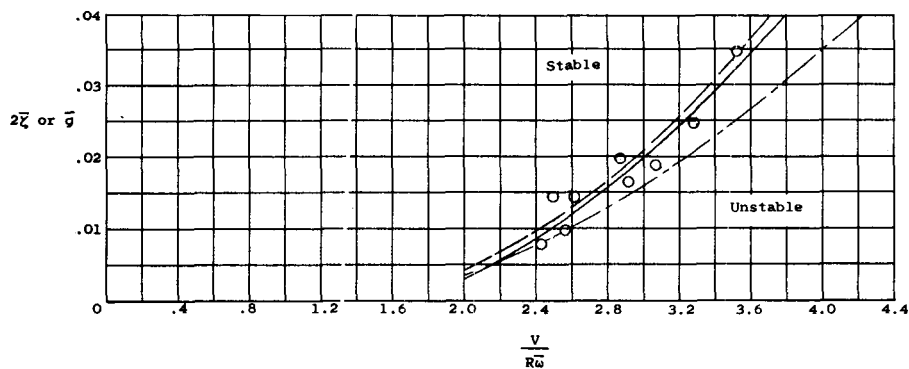
(c) $\beta_{0.75R} = 46^{\circ}$.

Figure 14.- Comparison of experimental whirl-flutter boundaries with theoretical boundaries based on measured static derivatives with viscous or structural damping. $l_0/R = 0.346$.
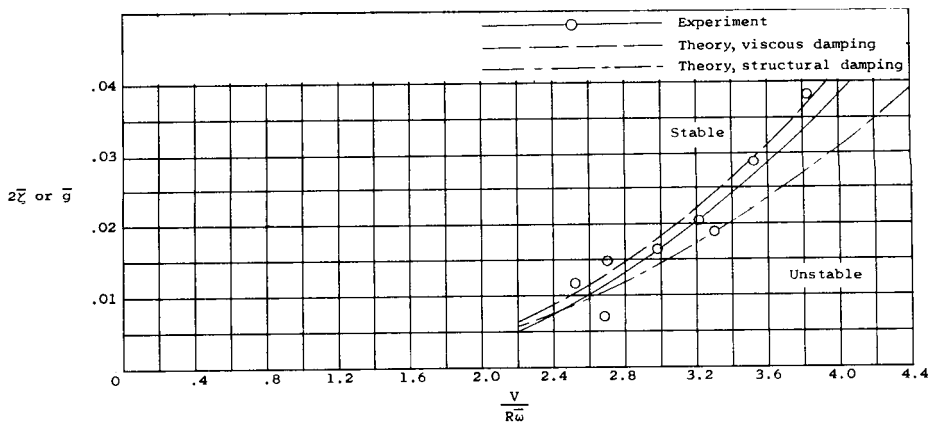
(d) $\beta_{0.75R} = 52^{\circ}$.
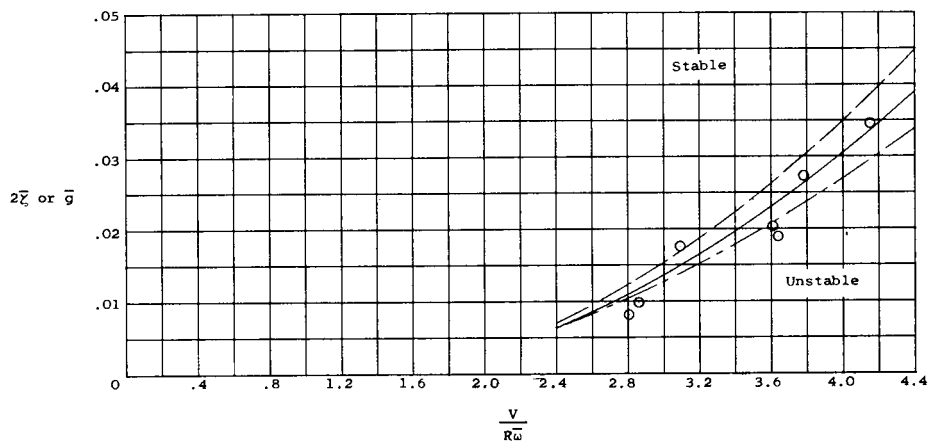
(e) $\beta_{0.75R} = 58^{\circ}$.

Figure 14.- Concluded.
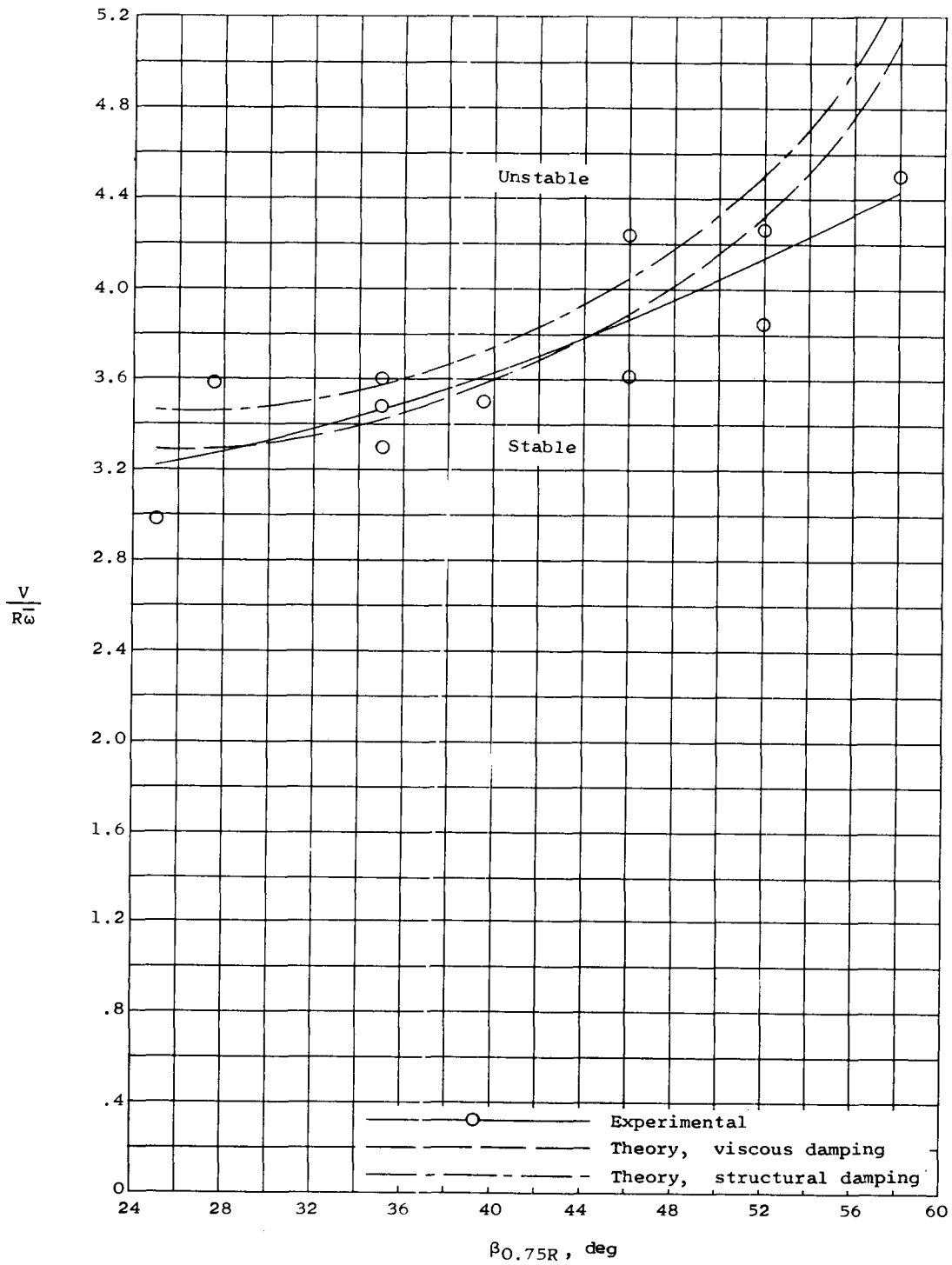
Figure 15.- Comparison of experimental whirl-flutter boundaries with theoretical boundaries based on measured static derivatives with viscous or structural damping. $l_0/R = 0.691$; $2\bar{\zeta}$ or $\bar{g} = 0.0059$.
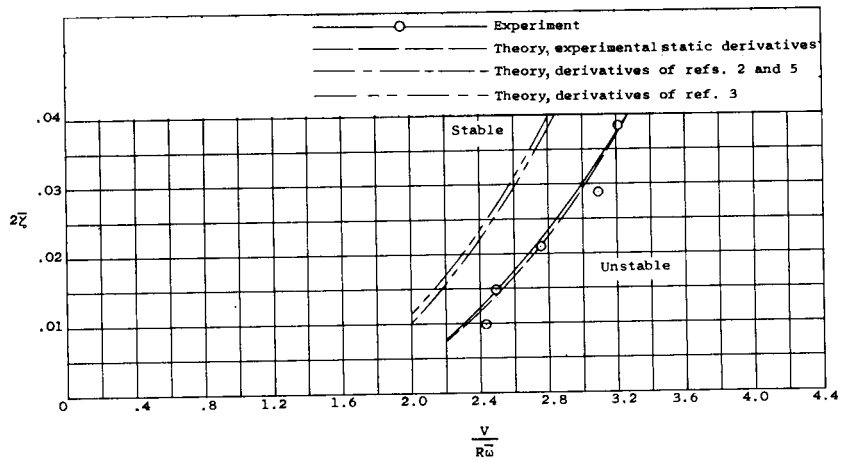
(a) $\beta_{0.75R} = 25°$.
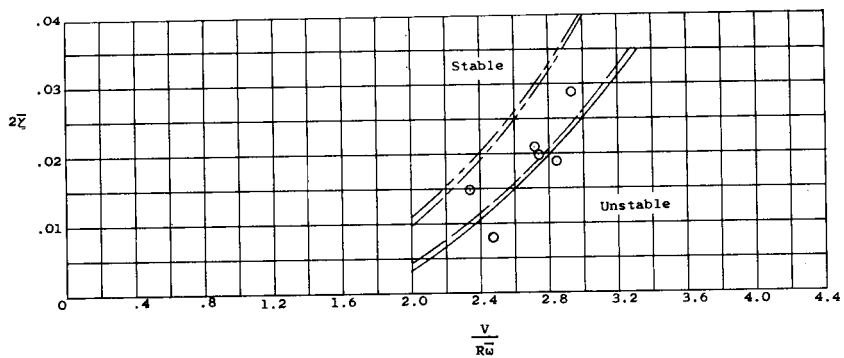
(b) $\beta_{0.75R} = 35°$.
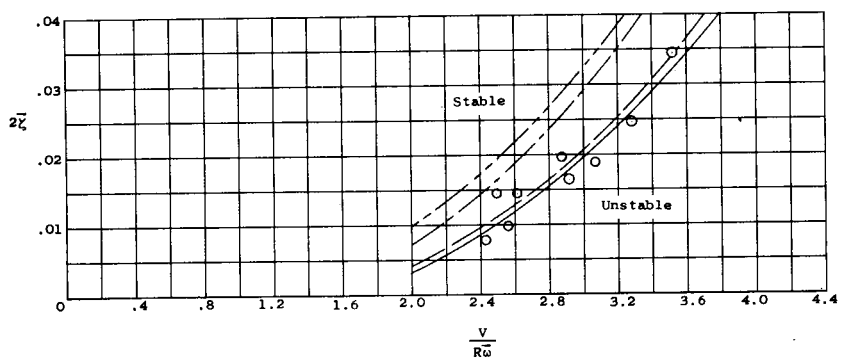
(c) $\beta_{0.75R} = 46°$.

Figure 16.- Comparison of experimental whirl-flutter boundaries with theoretical boundaries based on various aerodynamic derivatives with viscous·damping. $l_0/R = 0.346$.

Experiment
Theory, experimental static derivatives
Theory, derivatives of refs. 2 and 5
Theory, derivatives of ref. 3

Stable

Unstable

$2\bar{\zeta}$

.04

.03

.02

.01

0   .4   .8   1.2   1.6   2.0   2.4   2.8   3.2   3.6   4.0   4.4

$\dfrac{V}{R\omega}$

(d) $\beta_{0.75R} = 52^{\circ}$.

Stable

Unstable

$2\bar{\zeta}$

.05

.04

.03

.02

.01

0   .4   .8   1.2   1.6   2.0   2.4   2.8   3.2   3.6   4.0   4.4

$\dfrac{V}{R\omega}$

(e) $\beta_{0.75R} = 58^{\circ}$.

Figure 16.- Concluded.

Figure 17.- Comparison of experimental whirl-flutter boundaries with theoretical boundaries based on various aerodynamic derivatives with viscous damping. $l_o/R = 0.691$; $2\overline{\zeta} = 0.0059$.
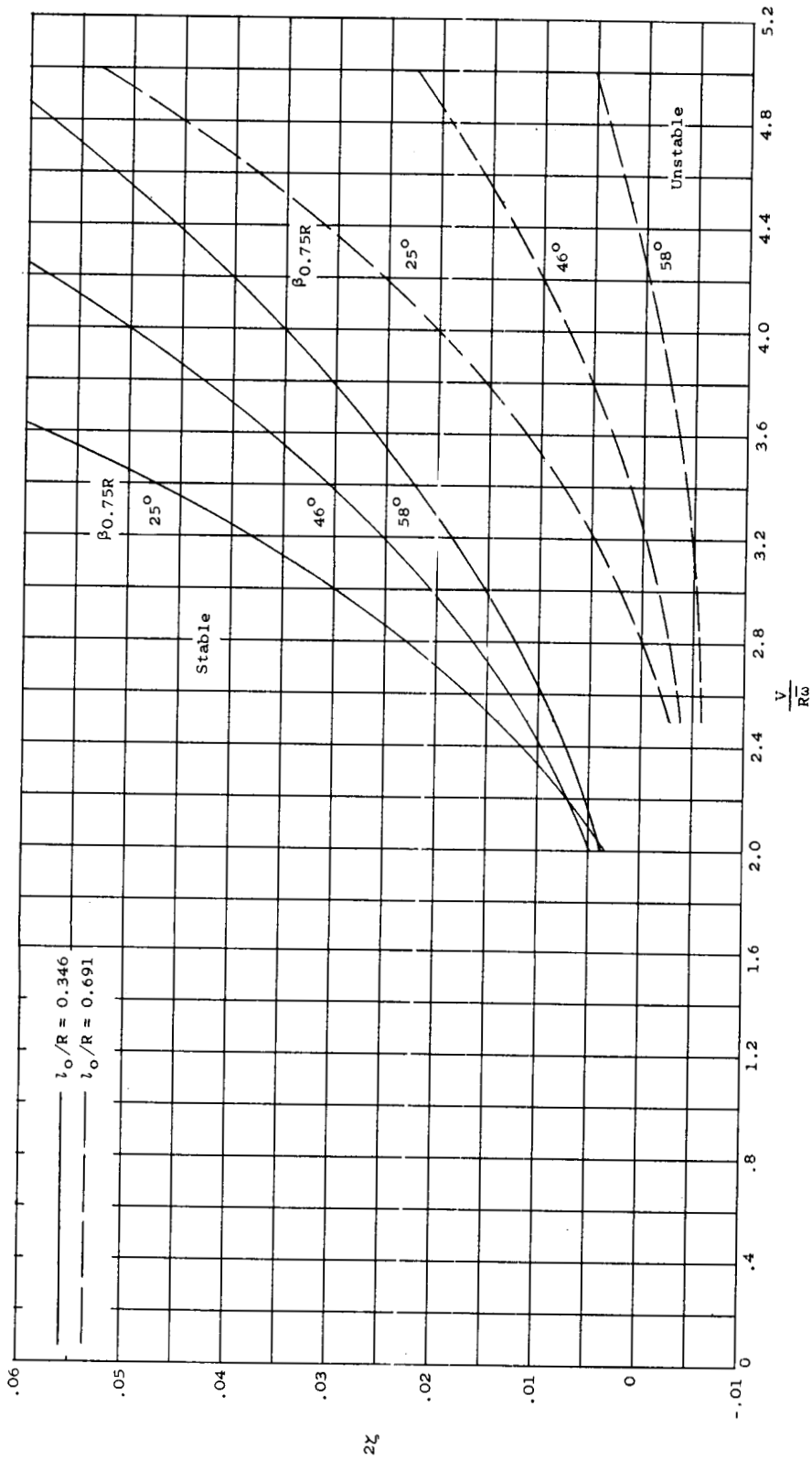
Figure 18.— Comparison of theoretical whirl-flutter boundaries for $l_o/R = 0.346$ and $l_o/R = 0.691$ based on measured static derivatives and viscous damping.

Experiment

$2\zeta = 0.010$, $l_o/R = 0.346$
$2\zeta = 0.025$, $l_o/R = 0.346$
$2\zeta = 0.0059$, $l_o/R = 0.691$
Faired curve

Theory

Reference 5
Reference 3

$\beta_{0.75R}$

C_{m_q}
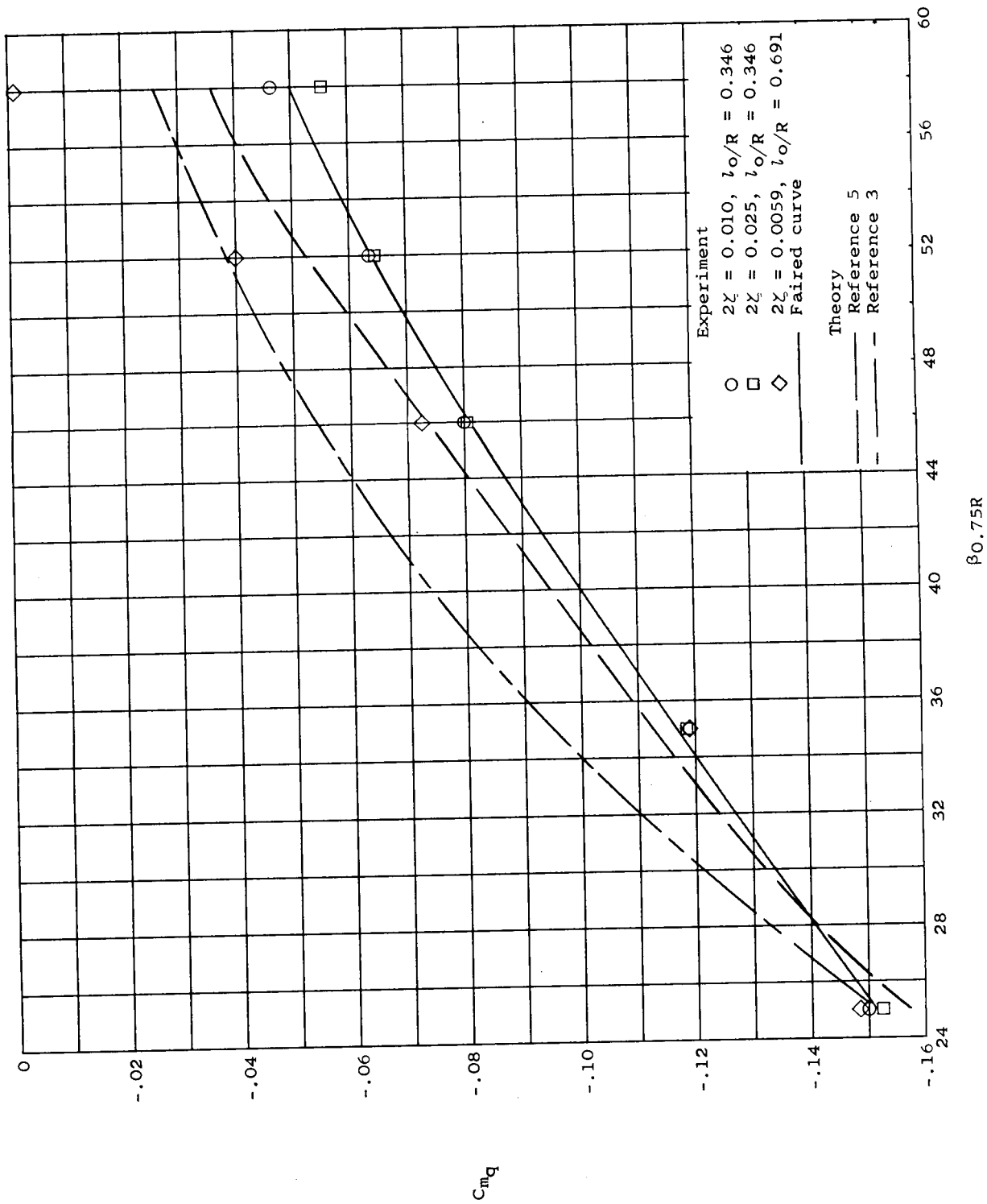
Figure 19.- Comparison of C_{m_q} inferred from measured whirl speeds with C_{m_q} derived from theory.

46
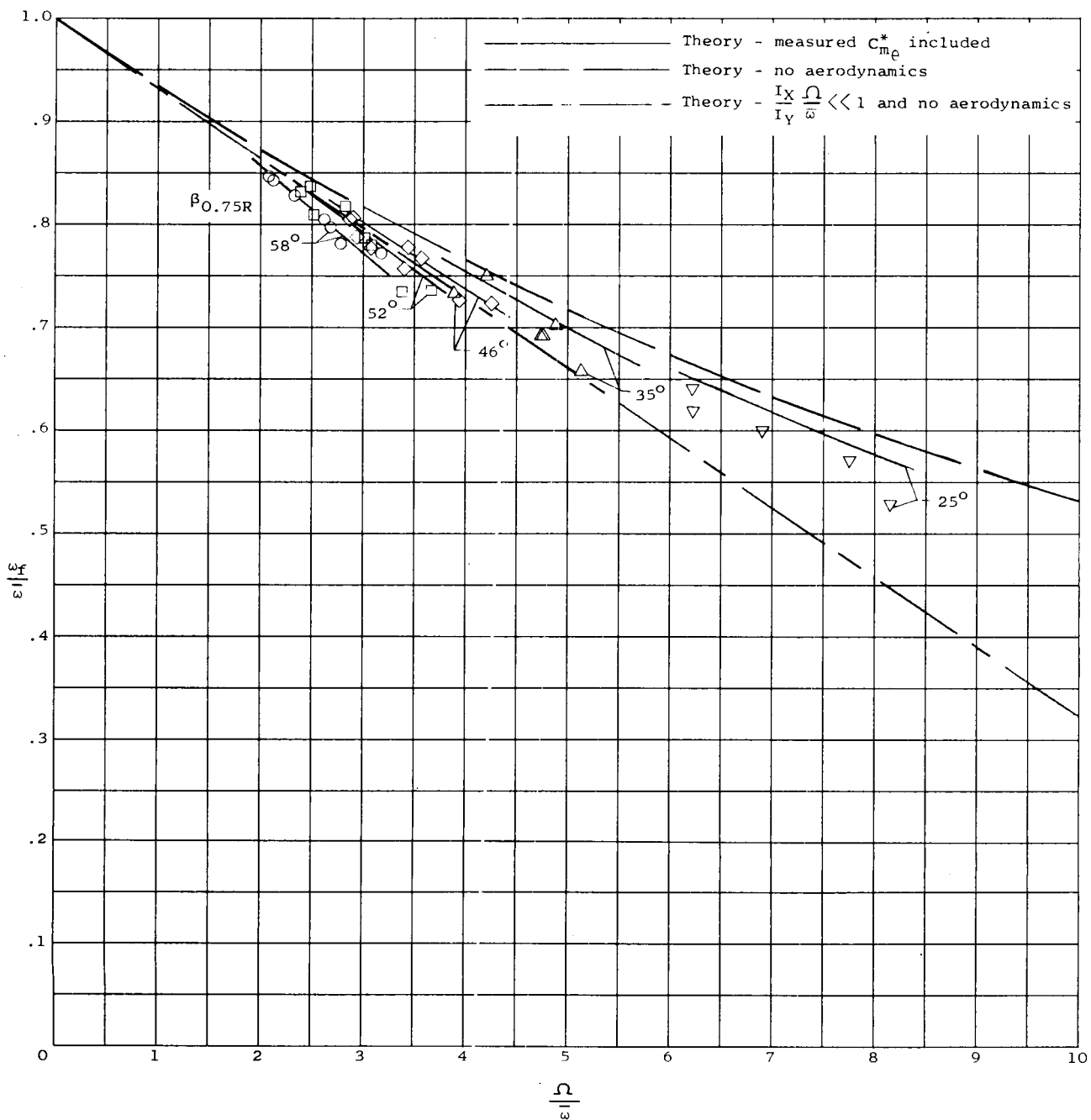
(a) $l_0/R = 0.346$.

Figure 20.- Comparison of experimental and theoretical whirl-flutter frequency ratios. Symbols indicate experimental frequency ratios.

47
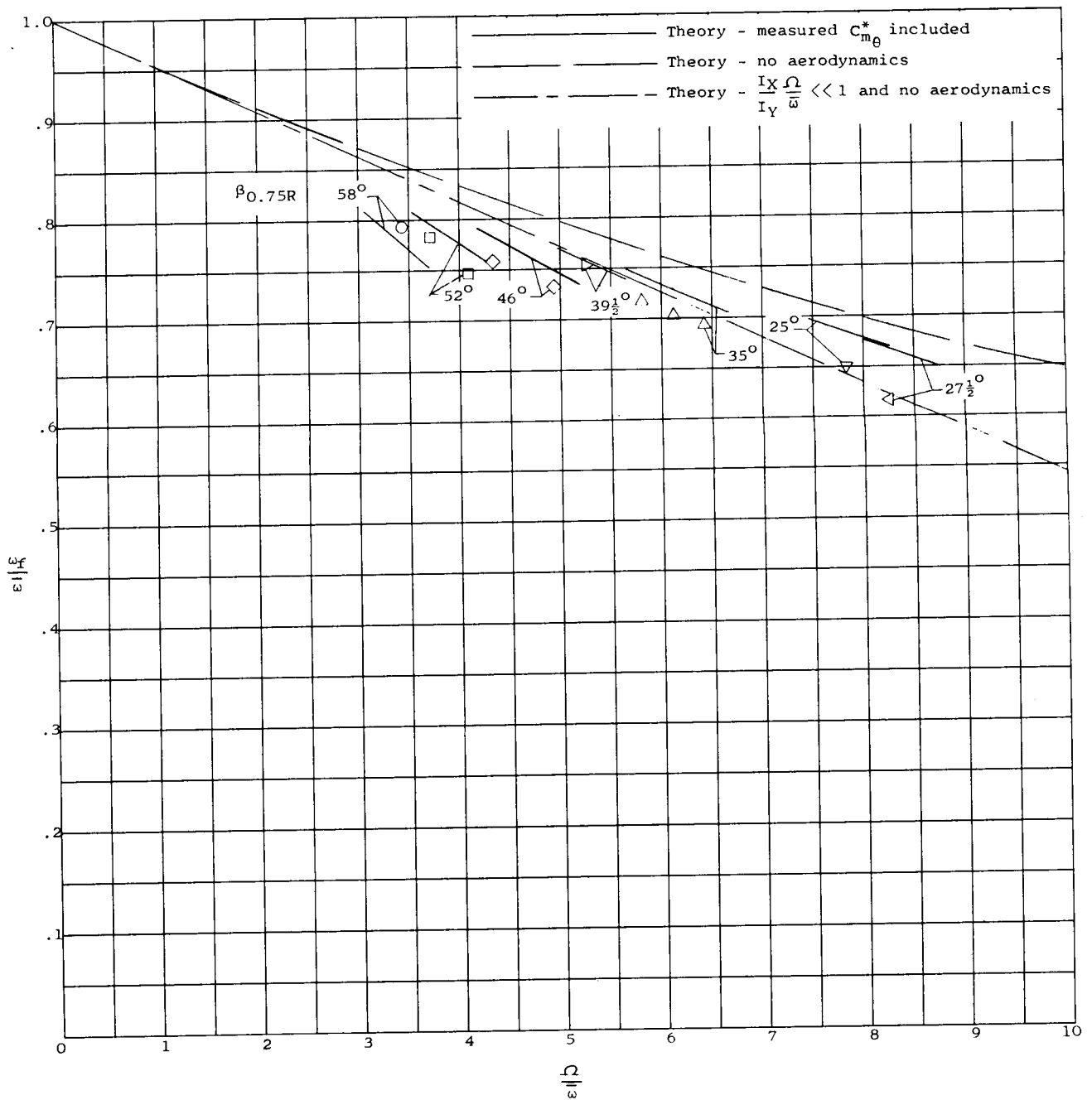
(b) $l_o/R = 0.691$.

Figure 20.- Concluded.
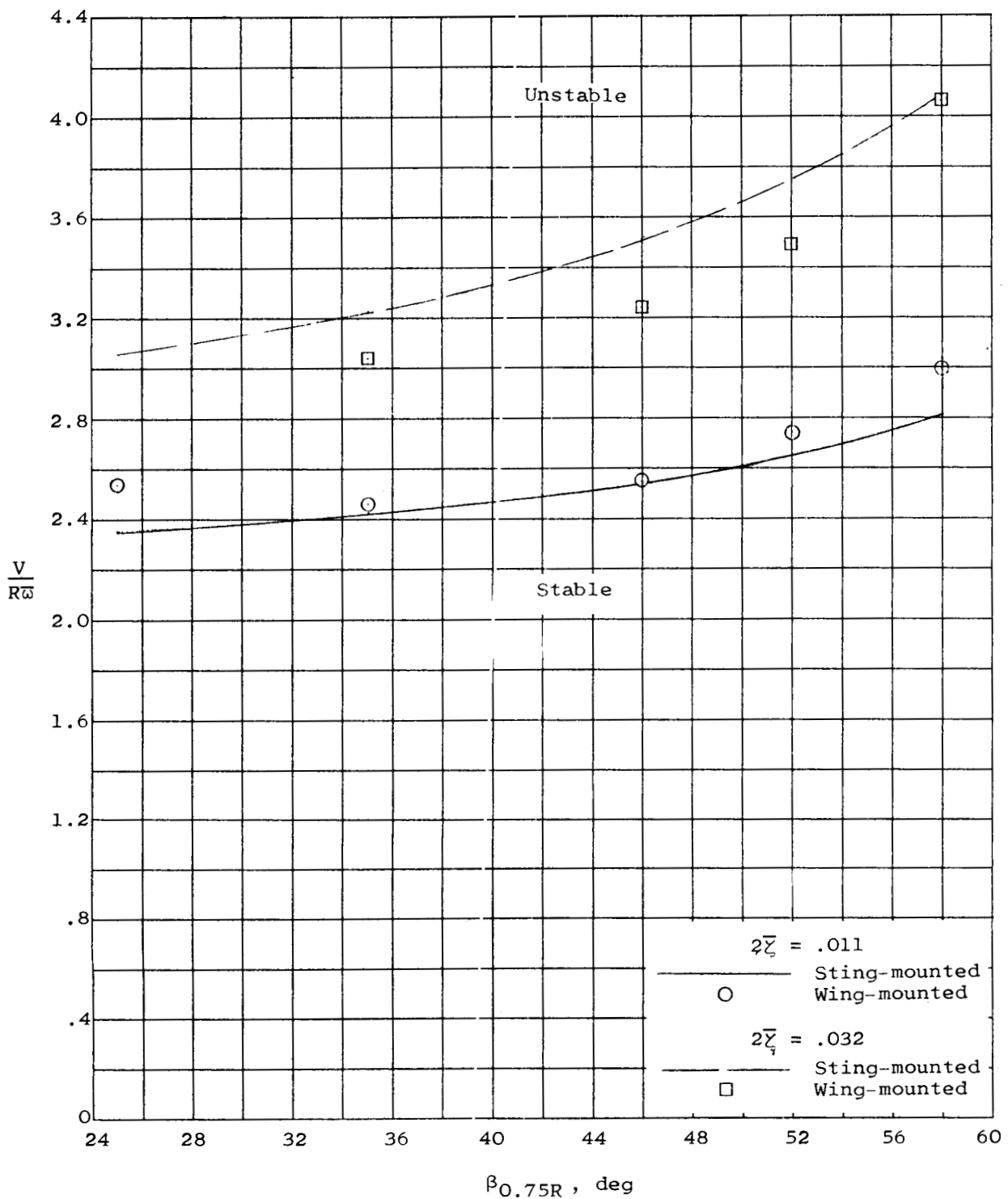
Figure 21.- Comparison of experimental whirl-flutter boundaries for the combination of propeller and power plant mounted on the sting and mounted on the cantilever wing. $l_0/R = 0.346$.
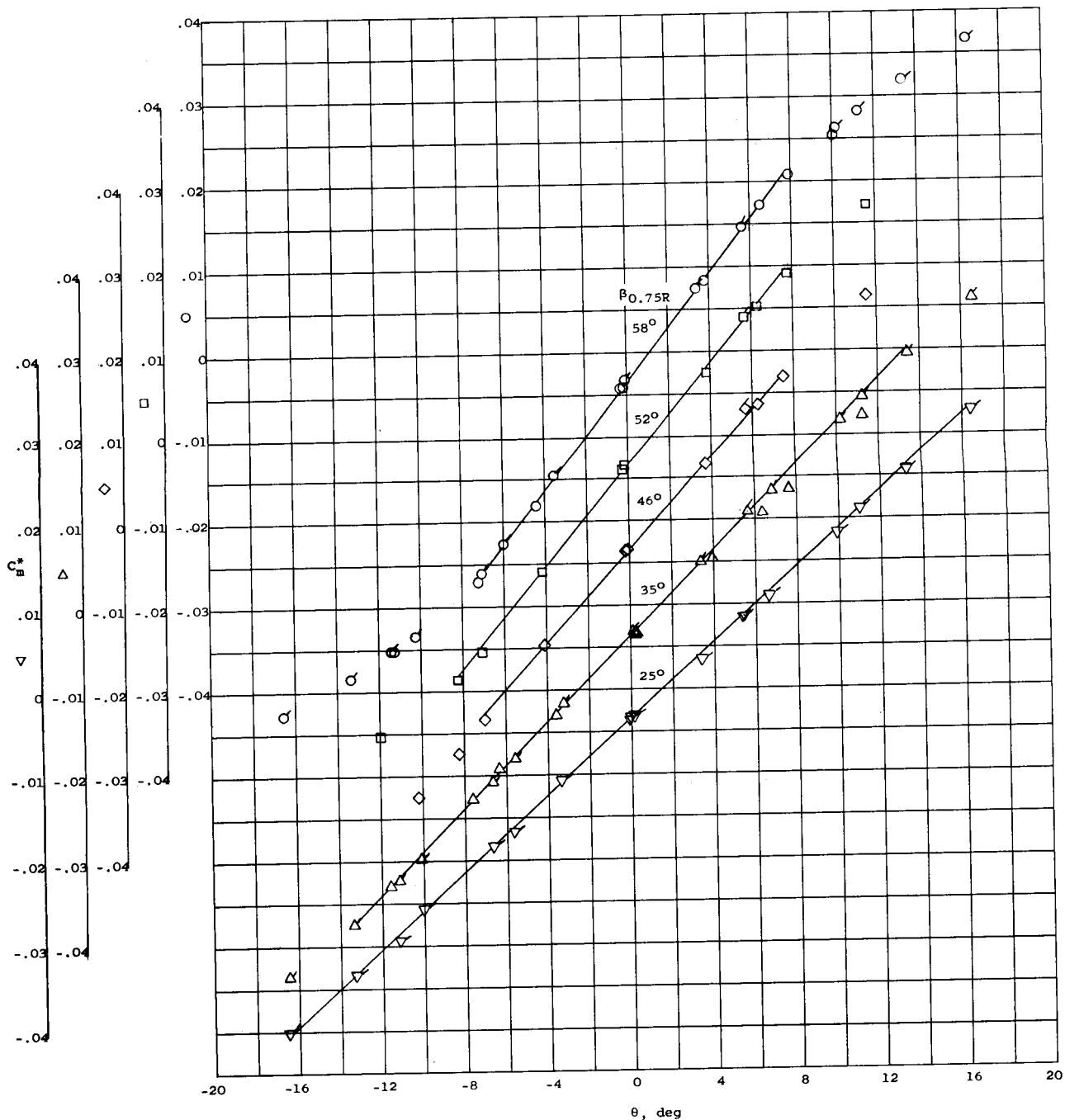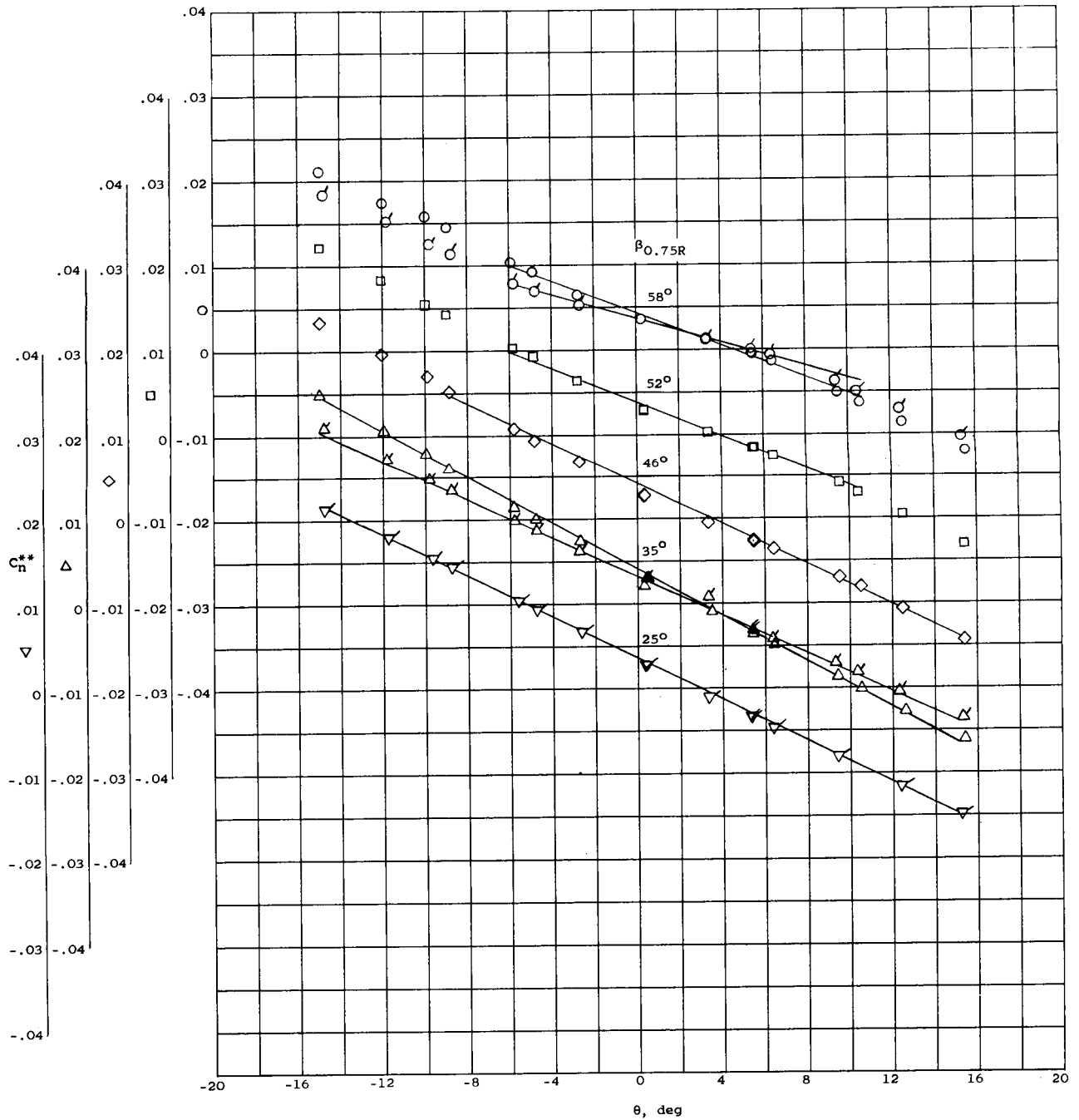
(a) Pitching moment. $l_0/R = 0.691$.

Figure 22.- Total moment coefficient about gimbal axis as a function of pitch angle for several blade angles. Plain symbols indicate data taken at a dynamic pressure of 100 lb/sq ft; flagged symbols, 50 lb/sq ft.
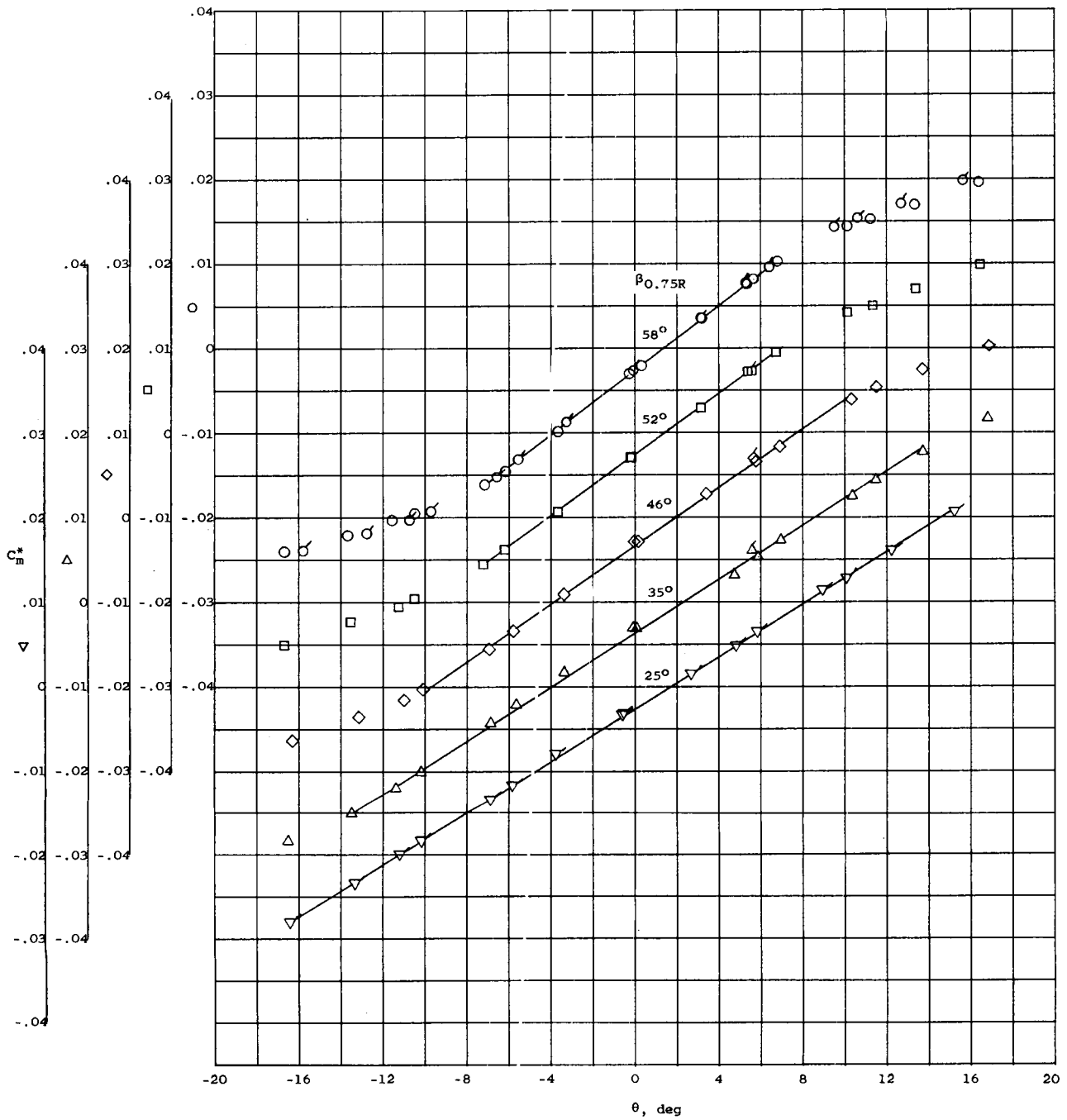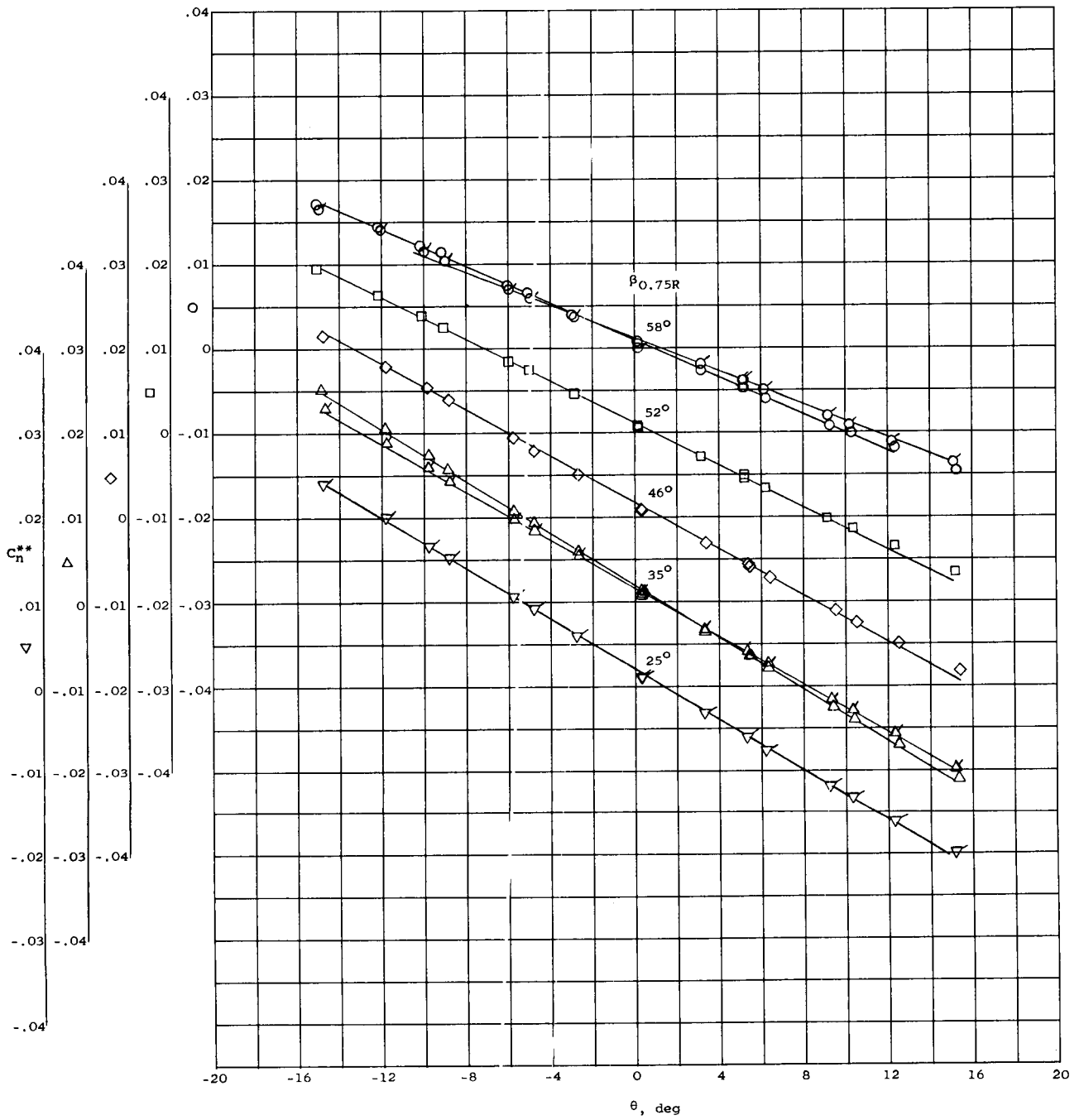
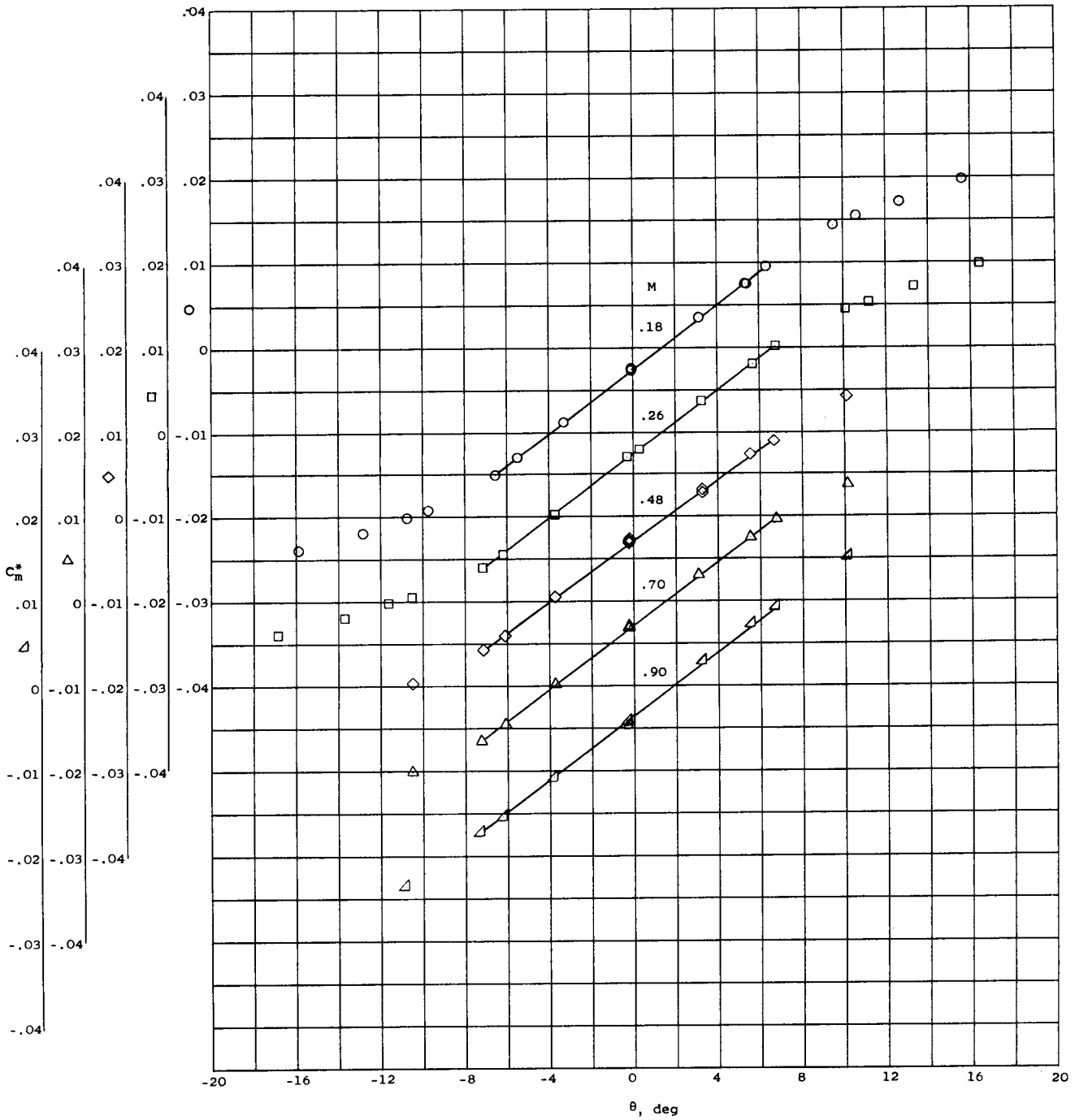(b) Pitching moment. $l_0/R = 0.346$.

Figure 22.- Continued.

(c) Yawing moment. $l_o/R = 0.691$.
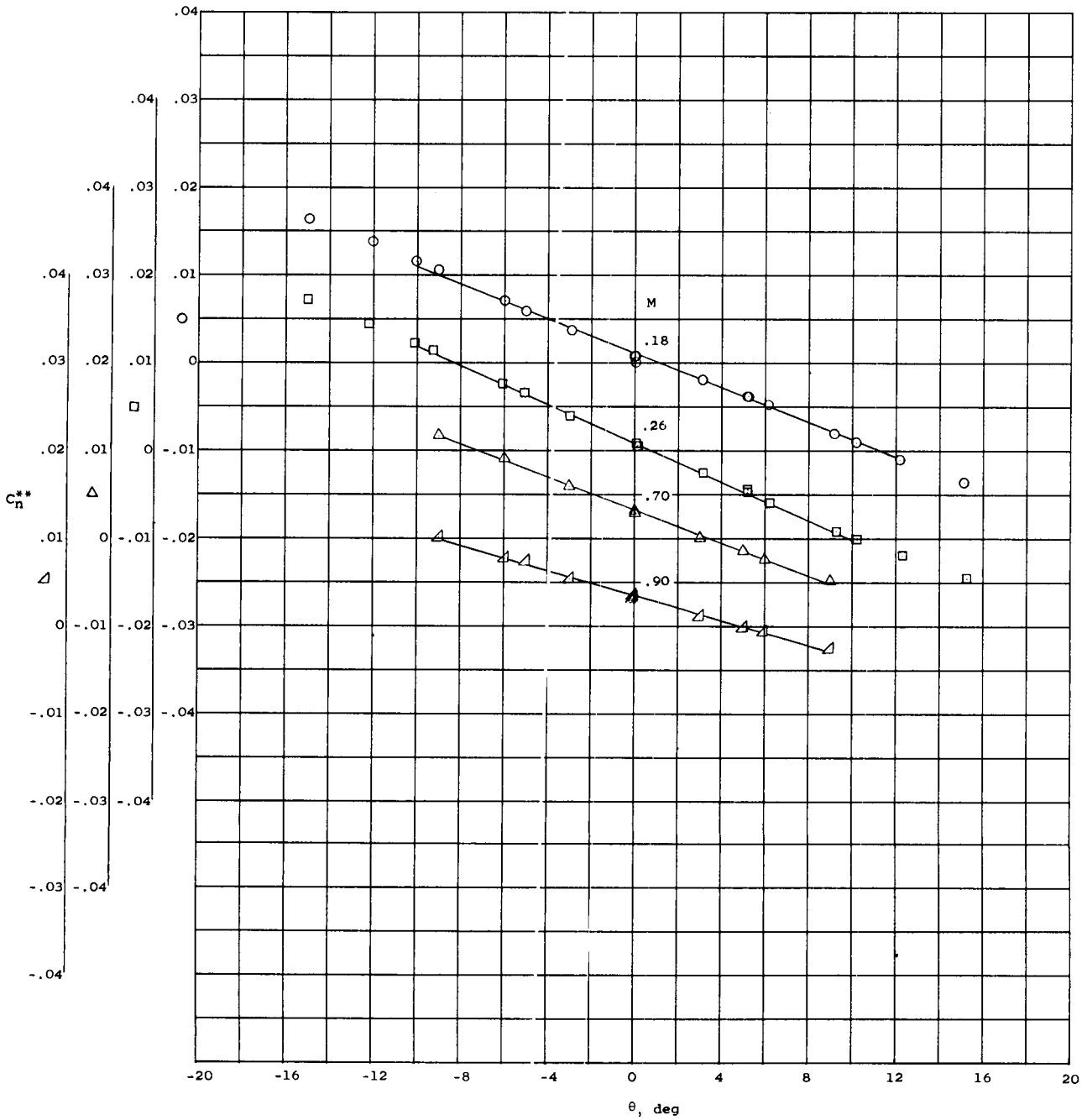
Figure 22.- Continued.

(d) Yawing moment. $l_0/R = 0.346$.

Figure 22.- Concluded.

(a) Pitching moment.

Figure 23.- Total moment coefficient about gimbal axis as a function of pitch angle for several Mach numbers. $l_0/R = 0.346$; $\beta_{0.75R} = 58°$.

(b) Yawing moment.

Figure 23.- Concluded.